Marine Environmental Research 216 (2026) 107891

Contents lists available at ScienceDirect

Marine Environmental Research

journal homepage: www.elsevier.com/locate/marenvrev

Relationships of the summer nutrient concentrations in the East China Sea with the Changjiang diluted water, upwellings and Kuroshio intrusion, from an interannual perspective

Qingling Zhang [a,b,1], Xinyan Mao [c,1], Yifei Luo [d], Xinyu Guo [d], Jie Shi [a,b,*]

[a] Key Laboratory of Marine Environment and Ecology, College of Environmental Science and Engineering, Ocean University of China, Ministry of Education, Qingdao, 266100, China
[b] Laboratory for Marine Ecology and Environmental Science, Qingdao Marine Science and Technology Center, Qingdao, 266237, China
[c] Key Laboratory of Physical Oceanography, College of Oceanic and Atmospheric Sciences, Ocean University of China, Qingdao, 266100, China
[d] Center for Marine Environmental Studies, Ehime University, Matsuyama, 790-8577, Japan

ARTICLE INFO

Keywords:
Nutrients
EOF analysis
Changjiang diluted water
Zhejiang coastal upwelling
Kuroshio intrusion

ABSTRACT

In summer, the East China Sea (ECS) faces ecological challenges like harmful algal blooms, hypoxia, and jellyfish blooms, linked to nutrient distributions influenced by Changjiang Diluted Water (CDW), Kuroshio intrusion, and Zhejiang Coastal Upwelling (ZCU). The inconsistent interannual variations of these processes complicate nutrient dynamics. This study used the Empirical Orthogonal Function (EOF) analysis to reveal the interannual variations (1993–2022) of summer dissolved inorganic nitrogen (DIN) and dissolved inorganic phosphorus (DIP) concentrations in the ECS. We demonstrated that interannual variability in southerly wind strength was a key regulator controlling the relative influence of CDW and ZCU on surface nutrients. Weaker southerly wind combined with stronger Changjiang discharge (e.g., 1999, 2002, 2020) enhanced the nearshore influence of CDW and reduced the ZCU intensity. This suppressed DIP supply and biological consumption of DIN, leading to accumulated surface DIN but depleted surface DIP in the Zhejiang Coastal (ZC) region. Conversely, stronger southerly wind combined with stronger Changjiang discharge drove the CDW moving offshore that increased offshore DIN concentrations. Simultaneously, the stronger southerly wind also intensified ZCU that enhanced coastal DIP supply and biological DIN uptake, resulting in reduced coastal surface DIN. Critically, we identify the distinct drivers for bottom DIP. Weaker ZCU led to increasing (decreasing) of bottom DIP concentrations in an area deeper (shallower) than 20 m, while stronger Kuroshio intrusion substantially boosted bottom DIP, influencing productivity in both ZC region and the East Zhejiang coastal (EZC) region. The intricate interplay of these physically driven nutrient fluxes, characterized by differing N/P ratios, underpinned the ECS's complex and variable summer nutrient structures with profound implications for understanding its ecological responses.

1. Introduction

The East China Sea (ECS), enclosed by the Chinese mainland, the Taiwan Island, the Korean Peninsula, the Kyushu Island of Japan, and the Ryukyu Islands, is recognized as one of the most productive marine ecosystems in the western Pacific Ocean (Chen and Wang, 1999; Heinze, 2014). In recent decades, increasing anthropogenic pressures have been placed on this ecologically significant region, manifested through frequent harmful algal blooms (HABs) (Wang et al., 2023), persistent jellyfish blooms (Xu et al., 2013), and expanding seasonal hypoxia events (Li et al., 2024a). These ecological issues have been fundamentally linked to variations in nutrient dynamics, particularly the changes of dissolved inorganic nitrogen (DIN) and dissolved inorganic phosphorus (DIP) concentrations (Chi et al., 2024). Alterations in nutrient regimes not only directly drive these phenomena but also exert cascading effects on higher trophic levels by influencing food web

This article is part of a special issue entitled: EBERCA published in Marine Environmental Research.

* Corresponding author. Key Laboratory of Marine Environment and Ecology, College of Environmental Science and Engineering, Ocean University of China, Ministry of Education, Qingdao, 266100, China.
E-mail address: shijie@ouc.edu.cn (J. Shi).

[1] These authors contributed equally to this work.

https://doi.org/10.1016/j.marenvres.2026.107891
Received 19 February 2025; Received in revised form 24 December 2025; Accepted 27 January 2026
Available online 28 January 2026

foundations and habitat suitability (Rattanarat et al., 2024). Consequently, comprehensive investigations of spatial and temporal distributions of nutrients in the ECS are essential for elucidating the underlying mechanisms of these ecological challenges and informing effective marine conservation strategies.

Globally, the distributions of nutrients in shelf seas have attracted considerable attentions. They are influenced by many factors, including various sources and complicated hydrodynamic processes in the ocean (Pereira et al., 2005; Rabouille et al., 2008; Luo et al., 2018; Lin et al., 2023). It was reported that river-borne nutrients significantly impact the structure and function of marine ecosystems in some shelf seas adjacent to North America and Europe (Conley et al., 2007; Guillaud et al., 2008; Kim et al., 2020). Riverine inputs significantly alter marine nutrient dynamics, modifying their spatial distributions and driving phytoplankton community shifts through changes in nutrient ratios (N:P:Si). However, in areas influenced by upwellings, deep cold and high-nutrient waters brought by upwelling acted as the key drivers of ecosystem changes (Brzezinski and Washburn, 2011; Sudheesh et al., 2017). These processes often co-occur, complicating distributions of nutrients in shelf seas. For instance, cross-shelf overturning and shelf-break downwelling hinder offshore nutrient transport (Yuan and Mitsudera, 2023), while cross-shore flows redistribute upwelled nutrients, regulating phytoplankton growth (Chabert et al., 2021). Additionally, river plumes can suppress coastal upwellings, altering nutrient availability (Wang and Yin, 2021).

In the ECS, nutrient distributions are governed by both external sources and complex hydrodynamic processes (Gao et al., 2015; Liu et al., 2017; Zhang et al., 2019). The most significant terrestrial source is the Changjiang River, whose nutrient fluxes have been profoundly altered by anthropogenic activities through agricultural, industrial, and urban development, profoundly affecting nutrient fluxes into the ECS (Liu et al., 2016, 2018). Since the 1960s, the Changjiang Diluted Water (CDW) has experienced rising DIN and declining dissolved silicate concentrations, altering estuary phytoplankton communities. This nutrient imbalance has caused coastal eutrophication, leading to increased red tides and hypoxic conditions in adjacent waters (Chai et al., 2006; Qu et al., 2019; Wang et al., 2021; Zhang et al., 2023). The intensity and the extensions of the CDW are influenced by the river discharges and wind fields, exhibiting maximum influence during summer (Bai et al., 2014; Hou et al., 2021).

The Kuroshio, a warm current, intrudes into the ECS from the area northeast of Taiwan, and then split into three branches: the surface Kuroshio Branch Current, the offshore Kuroshio Branch Current, and the nearshore Kuroshio Branch Current (Yang et al., 2012; Zhou et al., 2018; Li et al., 2024b). The intrusion of Kuroshio brings abundant nutrients and influences their distribution pattern in the ECS (Chen, 1996; Yang et al., 2018; Wang et al., 2022). Originating from the Kuroshio Subsurface Water (KSSW), the nearshore Kuroshio Branch Current is characterized by its lower temperatures, high salinity and high DIP concentrations at the bottom layer. In summer, it can reach nearshore areas at its strongest (Xu et al., 2018). Additionally, the Zhejiang Coastal Upwelling (ZCU) exhibits seasonal variations with a strongest intensity in summer (Wang and Wang, 2007; Xiao et al., 2024). The ZCU brings DIP-rich water from the Kuroshio to the coastal surface layer, enhancing the primary production. (Chen et al., 2004; Yang et al., 2013; Peng et al., 2023; Wei et al., 2024).

In summary, the CDW, the Kuroshio intrusion, and the ZCU constitute three fundamental processes governing nutrient distributions in the ECS. During summer, due to their concurrent operation with distinct interannual variations (Zhang et al., 2014; Luo et al., 2023), the examination of individual factors in isolation fails to provide a comprehensive representation of distributions of nutrients at interannual scales. Furthermore, the characterization of their complex interactions presents an even greater challenge in quantitative assessment. On the interannual timescales, the primary drivers of nutrient concentrations variations, the distinct regions dominated by each process, and their synergistic effects on nutrients and primary production remain poorly understood.

To address these gaps, we combined numerical modeling with statistical analysis to investigate the interactive regulation of nutrient distributions by the CDW, ZCU, and Kuroshio intrusion. Specifically, a three dimensional physical and biochemical coupled model was used to simulate the distributions of DIN and DIP concentrations in the ECS from 1993 to 2022. The model results in July were derived to establish a 30-year dataset in summer. By applying the Empirical Orthogonal Function (EOF) analysis method, we analyzed the interannual variations in DIN and DIP concentrations at both surface and bottom layers. Further investigation focused on uncovering the underlying hydrodynamic (e.g., CDW, Kuroshio intrusion, ZCU) and biological processes driving these variations. The primary objective of this study is to elucidate how the CDW, ZCU, and Kuroshio intrusion characterized by various nutrient ratios (N/P) interactively regulate the spatial and interannual variations in nutrient distributions. We thereby seek to offer critical insights for explaining and predicting the corresponding ecological challenges such as HABs, hypoxia, and jellyfish blooms, and contribution to the management of coastal seas.

2. Data and methods

2.1. Model description and configurations

The three-dimensional lower trophic biophysical model used in this study consists of two modules (Zhao and Guo, 2011). The physical module is based on the Princeton Ocean Model (Blumberg and Mellor, 1987; Mellor, 2003), which has been used in research in the East China Seas (Guo et al., 2006; Wang et al., 2008). This module provides water temperatures, current velocities, and turbulent viscosity coefficient to the biochemical module. The biochemical module is based on the biological part of the NORWECOM (Skogen and Søiland, 1998). There are seven state variables in the biochemical module: DIN, DIP, silicate, diatom, flagellate, detritus, and biogenic silica. The biochemical module simulates key biogeochemical processes including phytoplankton growth (consuming nutrients), respiration, mortality leading to detritus formation, settling of detritus to the seabed, resuspension of benthic detritus back into the water column, and remineralization of detritus into inorganic nutrients. The biomasses of diatom and flagellate (unit: mg N/m^3) were converted to be the Chlorophyll-a (Chl-a) concentrations (unit: mg Chl/m^3) using a nitrogen-to-chlorophyll ratio of 8 mg N/mg Chl within the range of 8–11 mg N/mg Chl ratio applied in studies of the regional seas of China (Zhao and Guo, 2011). The model has a horizontal resolution of 1/18° and 21 sigma levels vertically. Its domain (117.5°–131.5°E and 24°–41°N) covers the Bohai, Yellow, and ECS (Fig. 1a). In this study, the ECS is the primary study area, with its domain spanning 119°–126° E and 24°–33.5° N (Fig. 1b). Detailed information about this model have been given in previous research (Zhao and Guo, 2011; Wang et al., 2018a, 2019). The study period spans from 1993 to 2022, and July was regarded to be the representative month of summer when both ZCU prevails and the Changjiang discharge reaches its peak value (Siswanto et al., 2008; Xiao et al., 2024).

In this study, the climatological results on January 1st from Luo et al. (2023) were used as the initial conditions. And the model integrated from 1993 to 2022, driven by the forcing data in this period. Only the atmospheric forcing, runoff of the Changjiang River and the open boundaries data were set as interannual variations from 1993 to 2022, and the other forcing data were set to constants. Atmospheric forcing was derived from the European Centre for Medium-Range Weather Forecasts (ECMWF) ERA5 reanalysis data (https://cds.climate.copernicus.eu/cdsapp#!/dataset/reanalysis-era5-single-levels?tab=overview), which included evaporation, precipitation, heat fluxes, sea surface pressure, sea surface temperatures (SST), and 10 m wind speed. The monthly runoffs of ten rivers were from the River Sediment Bulletin of China (http://www.mwr.gov.cn/). And the riverine nutrient concentrations of the Changjiang River were 118.40 mmol/m^3 for DIN,

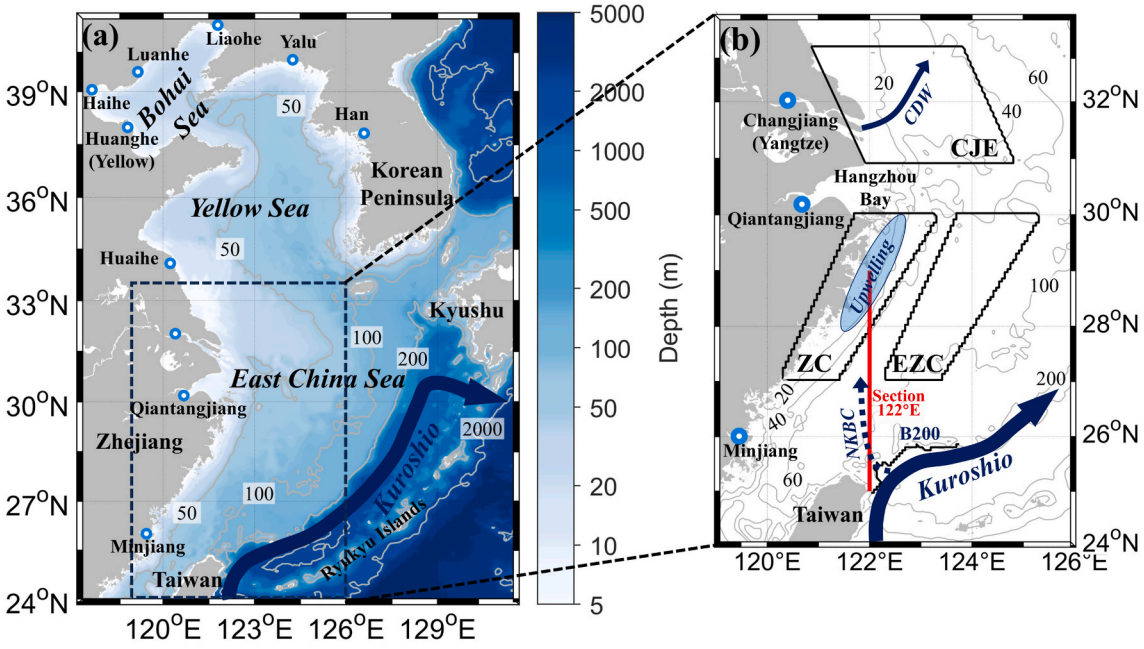

Fig. 1. The model domain (a) and the study area (b). In (a) and (b), bule-white dots are the positions of inflow from rivers, the dark blue thick arrows indicate the path of Kuroshio, and the gray lines represent the isobaths. In (b), the ZC, EZC, CJE, CDW and NKBC represent the Zhejiang coastal region, the East Zhejiang coastal region, the Changjiang Estuary, the Changjiang Diluted Water, and the Nearshore Kuroshio Branch Current. Section B200 is the location where NKBC intrudes into the ECS. Section 122°E is a section along 122°E from 25° to 29°N.

1.30 mmol/m^3 for DIP and 138.30 mmol/m^3 for silicate according to observations (Liang and Xian, 2018). The monthly open boundaries data were obtained from the results of an assimilative model from the Japan Coastal Ocean Predictability Experiment (JCOPE2; Miyazawa et al., 2009), which included sea levels, water temperatures, salinities, and velocities. The other forcing data were the same as Wang et al. (2019). And nutrient concentrations at the open boundaries were derived from the World Ocean Atlas 2005 (WOA 2005, https://www.nc ei.noaa.gov/products/world-ocean-atlas). Nutrient concentrations and phytoplankton biomasses at and east of the Taiwan Strait were obtained from the Japan Meteorological Agency (JMA) and field measurements by Chen and Wang (1999). Due to the limited data of the interannual variations of nutrient concentrations at the open boundaries, the climatologically monthly mean data were used in the model.

2.2. Observational data

This study uses satellite data and observation data to validate the model results. Satellite-derived Chl-a concentrations were acquired from NASA Ocean Color Level-3 products. Monthly data came from two sensors: the Sea-viewing Wide Field-of-view Sensor (SeaWiFS) at 9 km spatial resolution (1998–2002) and the Moderate Resolution Imaging Spectroradiometer (MODIS) at 4 km resolution (2003–2022) (https://oceancolor.gsfc.nasa.gov/l3/). To quantitatively validate simulated summer Chl-a concentrations, we interpolated satellite-derived Chl-a data into the model grids with the resolution of 1/18°. Satellite-derived Chl-a data in July from 1993 to 2022 were averaged to obtain a climatological distribution and to compare with the model results. These aligned datasets enabled comprehensive grid-point correlation analysis, with Pearson correlation coefficients quantifying model accuracy.

The observation data of temperatures, salinities, DIN and DIP concentrations in the ECS during summer were from available studies (Liu et al., 2010; Wang et al., 2011; Mi et al., 2012; Guo et al., 2014; Tseng et al., 2014; Jiang et al., 2015; Ye et al., 2015, 2017; Zhou et al., 2018; Lyu et al., 2020; Chen et al., 2021a; Yang et al., 2021; Wei et al., 2021). Modelled nutrient concentrations were spatially interpolated to exact observation coordinates, enabling point-to-point comparison where correlation coefficients were calculated to precisely quantify model performance.

2.3. EOF analysis method

The EOF analysis was employed to identify the dominant modes of spatiotemporal variations in DIN and DIP concentrations over the ECS continental shelf (depth <200 m). This technique is widely used to separate coherent spatial patterns and their temporal evolutions from multivariate environmental datasets, and has been widely applied in the analysis of spatiotemporal characteristics of atmospheric and oceanic variables (Baldacci et al., 2001; Brzezinski and Washburn, 2011; Wang et al., 2024; Zhang and Luo, 2024). Monthly anomaly fields for July (1993–2022) were computed by subtracting the climatological mean, effectively eliminating stationary background signals and seasonally recurrent patterns that could obscure interannual nutrient variability.

To investigate the mechanisms driving the dominant EOF modes of the summer nutrient concentrations, composite maps of physical and biochemical variables (DIN, DIP, Chl-a concentrations, water temperatures, and salinities) were created by averaging summer model results. We selected years with the principal component (PC) for a given mode exceeding +1 standard deviation from the mean values as the high years, while the years below −1 standard deviation were regarded as the low years. The averages for these years were named as High Maps and Low Maps, respectively. Their differences (High Maps minus Low Maps), referred to be Diff Maps, were calculated to highlight the spatial patterns associated with each EOF mode's variability.

3. Results

3.1. Distributions of physical and biochemical factors in the ECS during summer

The climatological distributions of physical and biochemical factors in summer were derived from the model results in July averaging from 1993 to 2022 (Figs. 2 and 3). The observational data in previous studies were also collected and overlapped with the modelled distributions

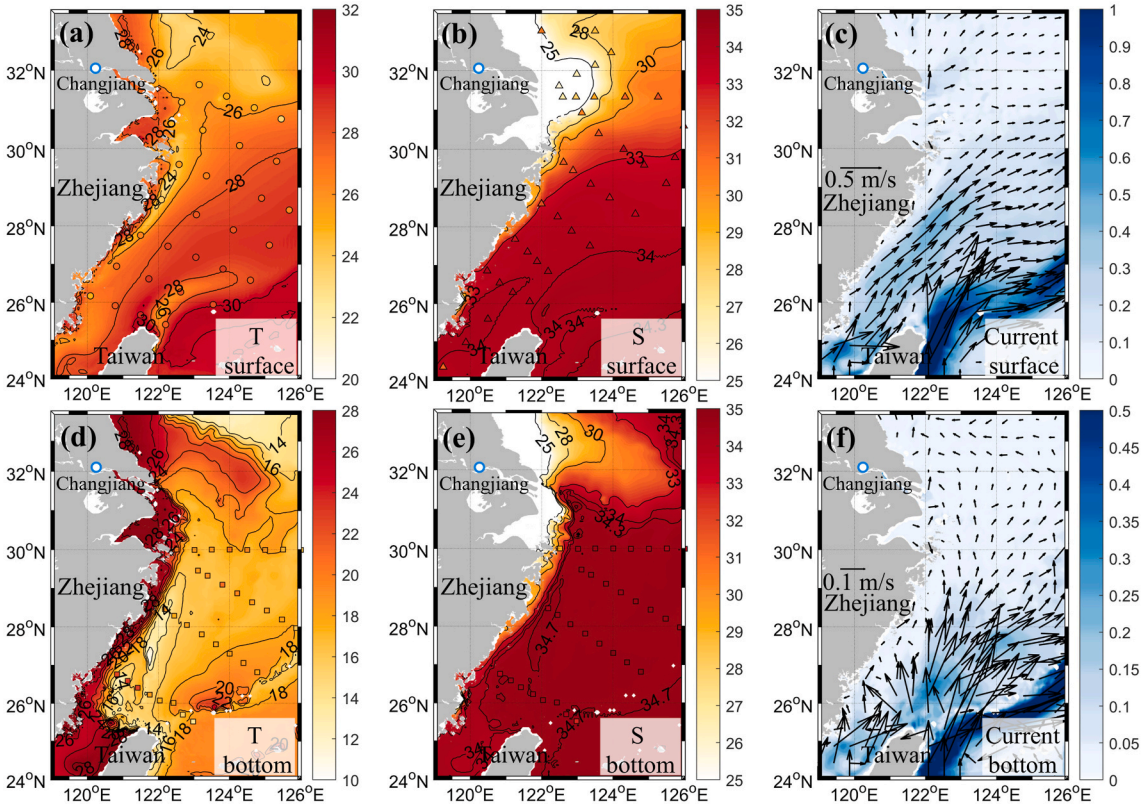

Fig. 2. The distributions of temperatures (T) (a, d), salinities (S) (b, e), and current (c, f) at surface (a–c) and bottom (d–f) of the ECS during summer. For areas deeper than 200 m, the data from the 200 m water layer is used. The scatters in (a, b, d, and e) denote sampling sites in the summer, and the color in scatters denotes the value of observations. The circles, squares, and triangles represent the observations of Chen et al. (2021a), Zhou et al. (2018), and Yang et al. (2021), respectively.

(scatters in Figs. 2 and 3). The results showed high consistency between the simulated and observed distributions, with correlation coefficients of 0.91 ($p < 0.01$, $n = 62$), 0.91 ($p < 0.01$, $n = 71$), 0.78 ($p < 0.01$, $n = 156$), and 0.82 ($p < 0.01$, $n = 80$) at the observation sites for temperatures, salinities, DIN, and DIP concentrations, respectively. The simulated distributions of Chl-a concentrations were validated by the satellite-derived data from MODIS-Aqua. The consistent spatial distributions (Fig. 3c–f) with the correlation coefficient of 0.81 ($p < 0.01$, $n = 15{,}750$) showed good agreement between simulated and observed monthly mean values in July. These comparisons indicated that the model successfully captured the characteristics of the observed spatial distributions in summer.

The surface distributions of temperature and salinity (Fig. 2a–c) indicated the main hydrodynamic processes in the study area. The warm and saline Kuroshio was indicated by the obviously high velocities larger than 0.80 m/s, flowing northeastward along the isobath of 200 m on the outer ECS continental shelf. Under the influence of southerly winds in summer, the CDW characterized by low sea surface salinities (SSS) expanded northeastward. At bottom, the water temperatures were lower and salinities were higher compared to those at the surface, which were consistent with the observations (Fig. 2d and e). The ZCU pumped deep cold water up to the surface to form a low-temperature band (<26 °C) at surface near the Zhejiang Coast (ZC) region, indicated by both the model results and observations (Fig. 2a). The cold and saline KSSW intruded into the ECS across the Section B200 (Fig. 1b) at bottom, indicated by a low-temperature (<16 °C) and high-salinity (>34.70) band extending from northeast of Taiwan to the ZC region along 122°E (Fig. 2d–f).

DIN concentrations at surface exhibited highly negative correlation with SSS (Figs. 2b and 3a). Near the Changjiang Estuary (CJE), the extension of the CDW indicated by low SSS resulted in the high DIN concentrations (>20 mmol/m^3). In the area south of 30°N, DIN concentrations were lower than 1.00 mmol/m^3. The pattern of DIP concentrations at the surface was almost inverse to that of DIN (Fig. 3b). In the CDW-occupied area, DIP concentrations were lower than 0.10 mmol/m^3 due to the consumption by the growth of phytoplankton driven by the high N:P ratio of the CDW. DIN and DIP concentrations at bottom were higher than those at surface. The region with DIN concentrations higher than 5.00 mmol/m^3 and the DIP concentrations higher than 0.50 mmol/m^3, extended from northeast of Taiwan to the ZC region which was induced by the Kuroshio intrusion (Fig. 3d and e). Chl-a concentrations were high in the nearshore region and decreased seaward. The concentrations higher than 2.00 mg/m^3 appeared near the CJE and ZC regions, indicated by both the model results and satellite observations from SeaWiFS and MODIS (Fig. 3c–f).

3.2. *Interannual variations in DIN concentrations in summer*

To validate the modelled interannual variations in summer DIN concentrations from 1993 to 2022, the observations from various cruises during this period were collected and overlapped on the modelled distributions (Fig. 4). The overall correlation coefficient between model results and observations was 0.92 ($p < 0.01$, $n = 321$), which indicated the model reproduced the interannual variations in DIN concentrations in summer of the ECS.

EOF analysis was applied to the 30-year results of the surface and bottom DIN concentrations. The first four EOF modes explained 60.33 %, 19.73 %, 8.06 %, and 3.99 % of the total variance in surface DIN concentrations, respectively; 72.45 %, 6.03 %, 5.05 %, and 3.99 % of the total variance in bottom DIN concentrations, respectively. As the first two EOF modes (EOF1 and EOF2) together explained over 70 % of the total variance, these two dominant modes were analyzed below.

The EOF1 of surface DIN concentrations ($EOF1_{SN}$) showed coherent fluctuations along the coastal region, with the strongest signals near the CJE and Hangzhou Bay, extending southward along the ZC region

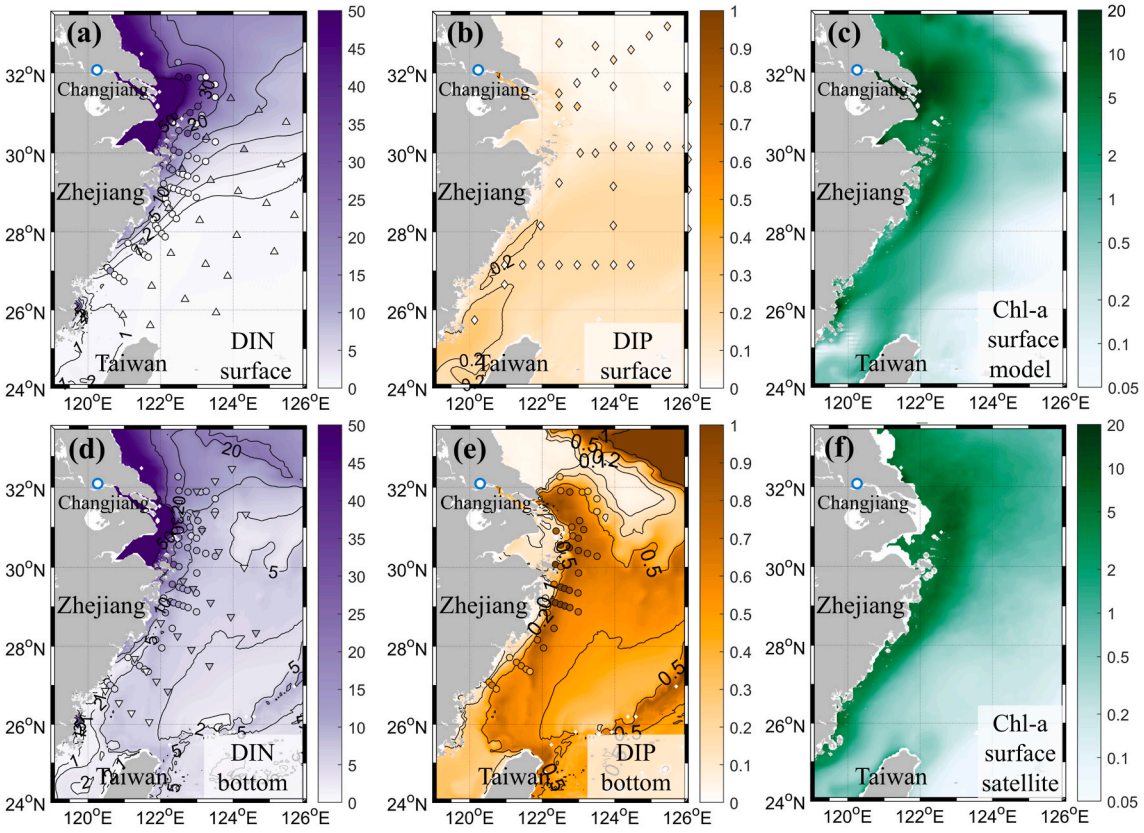

Fig. 3. The distributions of DIN (mmol/m^3, a, d), DIP (mmol/m^3, b, e) concentrations at surface (a, b) and bottom (d, e), and Chl-a concentrations at surface from model results and satellites (mg/m^3, c, f) of the ECS during summer. For areas deeper than 200 m, the data from the 200 m water layer is used. The scatters in (a, b, d, and e) denote sampling sites in the summer, and the color in scatters denote the value of observations. The circles, regular triangles, inverted triangles, and diamonds represent the observations of Wei et al. (2021), Liu et al. (2010), Lyu et al. (2020), and Ye et al. (2015), respectively.

(Fig. 5a). The principal component time series of the first EOF mode for surface DIN ($PC1_{SN}$) indicated that concentrations in these coastal areas were substantially higher than average during years when strong positive phases of this pattern (e.g., 1999, 2002, 2010, 2015, and 2020) (Fig. 5e).

The EOF2 of surface DIN ($EOF2_{SN}$) revealed a contrasting distribution between northern and southern regions of study areas (Fig. 5b). The principal component time series for the second EOF mode ($PC2_{SN}$) identified years when this pattern was dominant (e.g., 1995, 1996, 1998, 2010, 2016). During these years, DIN concentrations were higher than the average value in the offshore area next the CJE but lower than the average value along the ZC region (Fig. 5e).

The spatial distributions and temporal variations of bottom DIN concentrations were close to those at the surface (Fig. 5c, d, f). The strong correlation between surface and bottom variability ($r = 0.97$ for the EOF1, $r = 0.88$ for the EOF2) ($p < 0.01$) indicated that the same physical processes controlled the DIN distributions throughout the water column during summer.

3.3. Interannual variations in DIP concentrations in the ECS

The observational data of DIP concentrations were collected to validate the interannual results (Fig. 6). The correlation coefficient between simulations and observations was 0.53 ($p < 0.01$, $n = 234$), which was lower than that for DIN. DIP concentrations were much lower than those of DIN, which increased the challenge of accurate simulation of DIP. Especially in the coastal regions, the model struggled to capture the observed high values likely attributable to riverine inputs (Fig. 6g). There were also lower simulations than the observations at the bottom layer in some years (e.g., 2011). Except for these episodic observations, the model reproduced the observed interannual variations in DIP concentrations at both surface and bottom.

The first four EOF modes explained 58.72 %, 12.69 %, 5.27 %, and 3.90 % of the total variance in surface DIP concentrations, respectively; 42.02 %, 14.36 %, 10.24 %, and 5.83 % of the total variance in bottom DIP concentrations, respectively. Together, EOF1 and EOF2 accounted for more than half of variability of both surface and bottom DIP concentrations. Compared with DIN concentrations, the relatively low percentage explained by EOF1 and EOF2 indicated the complex temporal variations in DIP concentrations.

The spatial pattern of EOF1 for surface DIP ($EOF1_{SP}$) showed the strongest variation in the ZC region (28°N–31°N) where ZCU occupied and extended offshore (Fig. 7a). The time series of PC1 of surface DIP concentrations ($PC1_{SP}$) were nearly identical to the $PC1_{SN}$ ($r = 0.96$, $p < 0.01$) (Fig. 7e), indicating that DIN and DIP were governed by the same physical processes in this mode. The EOF2 for surface DIP ($EOF2_{SP}$) exhibited significant positive values along the ZC region (Fig. 7b). The time series of PC2 of surface DIP ($PC2_{SP}$) was similar to the $PC2_{SN}$ (correlation coefficient of 0.71, $p < 0.01$) (Fig. 7e), again suggesting a shared physical driver.

The spatial pattern of EOF1 of bottom DIP concentrations ($EOF1_{BP}$) showed a widespread increase in concentrations over most of the continental shelf during its positive phase, with only a small area of decrease along the ZC region (Fig. 7c). The time series of PC1 of bottom DIP concentrations ($PC1_{BP}$) was similar to the PC1 of bottom DIN concentrations ($r = 0.76$, $p < 0.01$). The spatial pattern of EOF2 of bottom DIP concentrations ($EOF2_{BP}$) revealed a clear band of high values extending from the northeast Taiwan to the ZC region and then eastward (Fig. 7d), closely following the known intrusion path of the Kuroshio. The time series of PC2 of bottom DIP concentrations ($PC2_{BP}$) showed that the

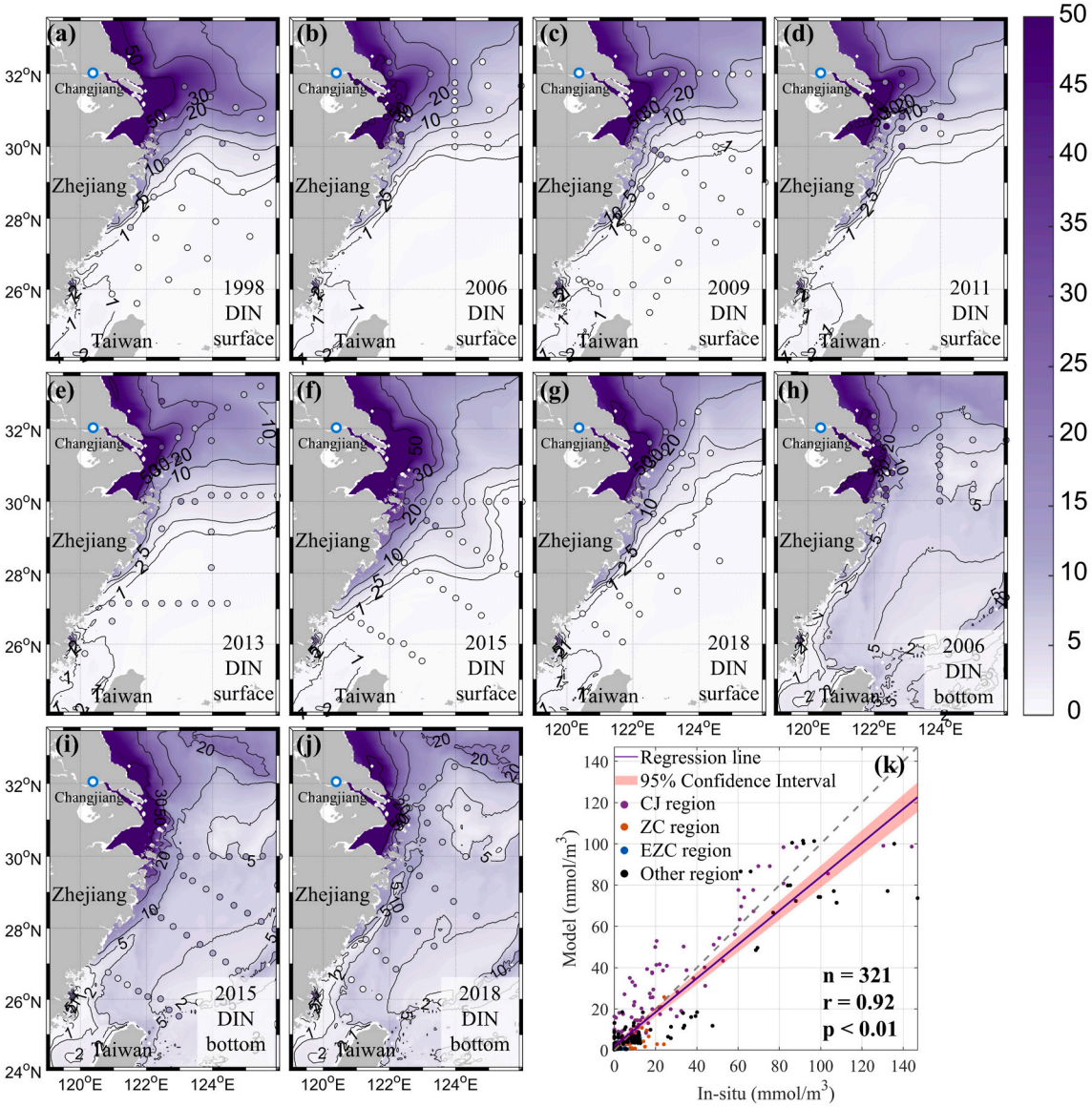

Fig. 4. Validations of the modelled interannual variations in DIN concentrations in summer (mmol/m^3). The scatters denote sampling sites in the summer, and the color in scatters denote the value of observations (Liu et al., 2010; Wang et al., 2011; Guo et al., 2014; Tseng et al., 2014; Ye et al., 2015; Zhou et al., 2018; Lyu et al., 2020). The purple, red, blue, and black scattered dots in k represent CJ, ZC, EZC, and other regions, respectively. The specific regional divisions are shown in Fig. 1b.

influence of this Kuroshio-driven pattern suggested an increasing trend after 2016 (Fig. 7f).

4. Discussion

4.1. Processes influencing the interannual variations in DIN and DIP concentrations

To elucidate the physical mechanisms behind the dominant EOF modes of summer nutrients, high and low years were identified based on the PCs. Composite maps (High Maps and Low Maps) of nutrient concentrations, temperatures, salinities, and Chl-a concentrations were generated for these years, which were presented in the Supplementary material (Fig. S1–S8). As the spatial patterns among variables in these composite maps were similar, difference maps (Diff Maps; High minus Low Maps) were presented here to clearly analyze the contrasts and associated mechanisms (Figs. 8 and 9).

For the EOF1 of surface nutrients, $EOF1_{SN}$ and $EOF1_{SP}$ were controlled by the same factors as presented in Section 3.3. However, their Diff Maps exhibited opposite patterns (Figs. 8 and 9). Throughout the coastal areas, DIN concentrations were higher during high years, whereas DIP concentrations were lower (Figs. 8a and 9a). Concurrently, surface temperatures in the ZC region were higher during high years (Fig. 8b). The ZCU intensity, represented by the average July vertical velocity in the ZC region, showed significant negative correlations with the PC1 time series of surface nutrients ($r = -0.51$ for $PC1_{SN}$, $r = -0.54$ for $PC1_{SP}$), indicating a weaker ZCU during high years (Fig. 10a and Table 1). Near the CJE and the adjacent coastal areas to the south (29°–32°N), salinity was lower in high years. The PC1 time series correlated positively with July Changjiang discharge ($r = 0.74$ for $PC1_{SN}$, $r = 0.66$ for $PC1_{SP}$), indicating that higher discharge contributed to the lower salinity (Fig. 10b–Table 1). Moreover, there were significant negative correlations ($r = -0.61$ for $PC1_{SN}$, $r = -0.59$ for $PC1_{SP}$) between the PC1 of surface nutrients and the southerly wind strength associated with CDW extension (Bai et al., 2014), which explained the accumulation of low-salinity water nearshore (Moon et al., 2012).

CDW and ZCU are characterized by distinct nutrient ratios. The ZCU transports bottom water with a low N/P ratio (N/P = 10–11) (Wei et al.,

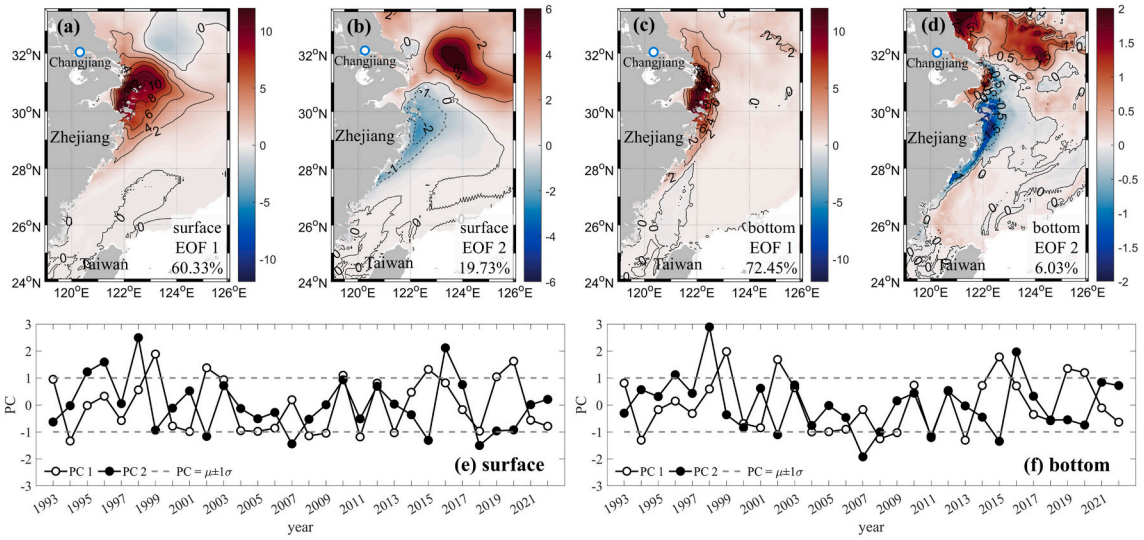

Fig. 5. The first EOF mode (EOF1) and second EOF mode (EOF2) of DIN concentrations at surface (a, b) and bottom (c, d) layer in summer, and their corresponding normalized principal component of EOF1 (PC1) and principal component of EOF2 (PC2) time series during 1993–2022 (e, f). The dashed lines in e and f represent PC = μ ± 1 σ.

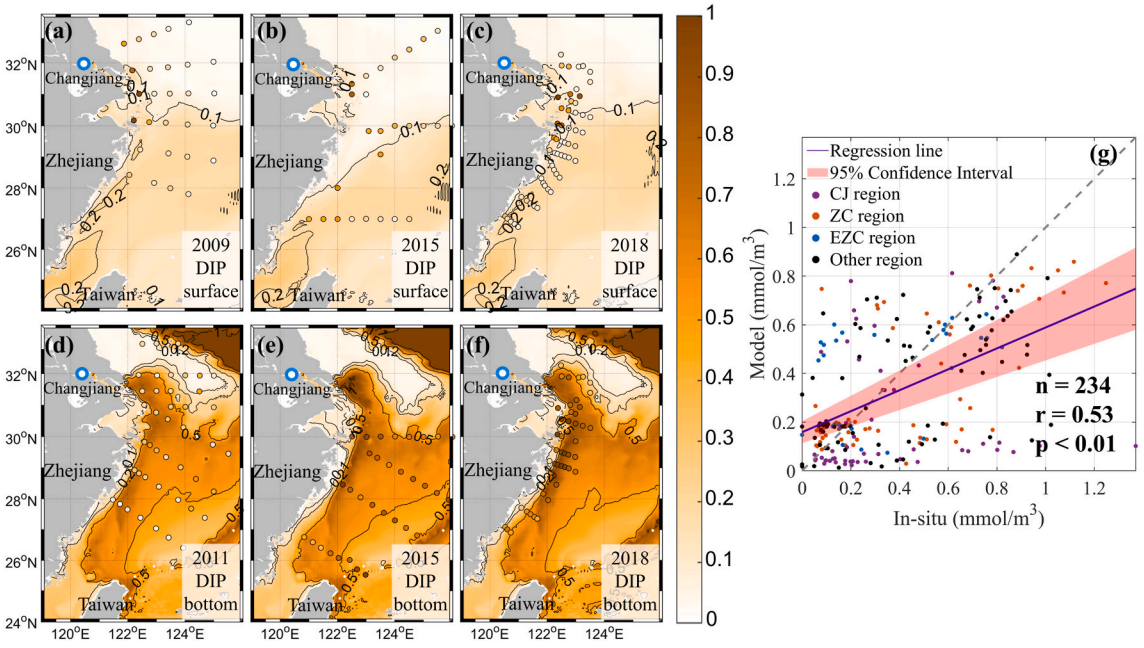

Fig. 6. Validations of the modelled interannual variations in DIP concentrations in summer (mmol/m^3). The scatters denote sampling sites in the summer, and the color in scatters denote the value of observations (Mi et al., 2012; Jiang et al., 2015; Ye et al., 2017; Zhou et al., 2018; Wei et al., 2021). The purple, red, blue, and black scattered dots in g represent CJ, ZC, EZC, and other regions, respectively. The specific regional divisions are shown in Fig. 1b.

2024) to the surface, supplying DIP and stimulating phytoplankton growth (Chen et al., 2017; Tseng et al., 2014; Wu et al., 2023). In contrast, the Changjiang delivers CDW with a high N/P ratio (N/P = 91 in this model), which also promotes phytoplankton growth (Sun et al., 2023). The Diff Maps of Chl-a (Figs. 8d and 9d) revealed that during high years, both weakened ZCU and enhanced Changjiang discharge influenced the coastal region. The weakened ZCU reduced DIP supply to the ZC region, limiting phytoplankton growth and thus surface DIN consumption. Meanwhile, the larger discharge and weaker southerly winds, CDW accumulated nearshore, increasing surface DIN supply. This stimulated phytoplankton growth, which in turn consumed more DIP.

For the EOF2 of surface nutrients, during high years, surface DIN concentrations were higher and DIP concentrations were lower in the offshore region northeast of the CJE region (north of 30°N), while DIN concentrations were lower and DIP concentrations were higher in the ZC region (28°–31°N) (Figs. 8e and 9e). Lower salinity offshore during high years was linked to higher July Changjiang discharge, as shown by positive correlations with PC2 (r = 0.46 for $PC2_{SN}$, r = 0.43 for $PC2_{SP}$; Table 2). The PC2 time series also correlated positively with the southerly wind strength (r = 0.50 for $PC2_{SN}$, r = 0.38 for $PC2_{SP}$; Table 2), indicating stronger winds drove greater northeastward CDW extension during high years. In the ZC region, lower temperatures and higher salinity during High years, alongside positive correlations between PC2 and ZCU intensity (r = 0.39 for $PC2_{SN}$, r = 0.49 for $PC2_{SP}$; Table 2), reflected the influence of a stronger ZCU. In addition, the higher salinity was also caused by the reduced southward presence of the CDW.

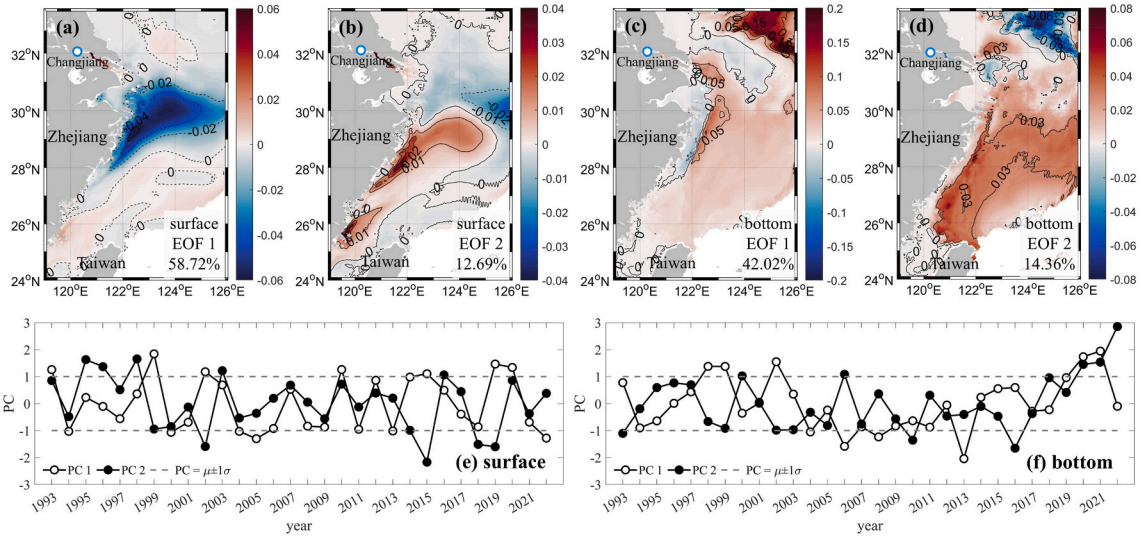

Fig. 7. The first EOF mode (EOF1) and second EOF mode (EOF2) of DIP concentrations at surface (a, b) and bottom (c, d) layer in summer, and their corresponding normalized principal component of EOF1 (PC1) and principal component of EOF2 (PC2) time series during 1993–2022 (e, f). The dashed lines in e and f represent PC = μ ± 1 σ.

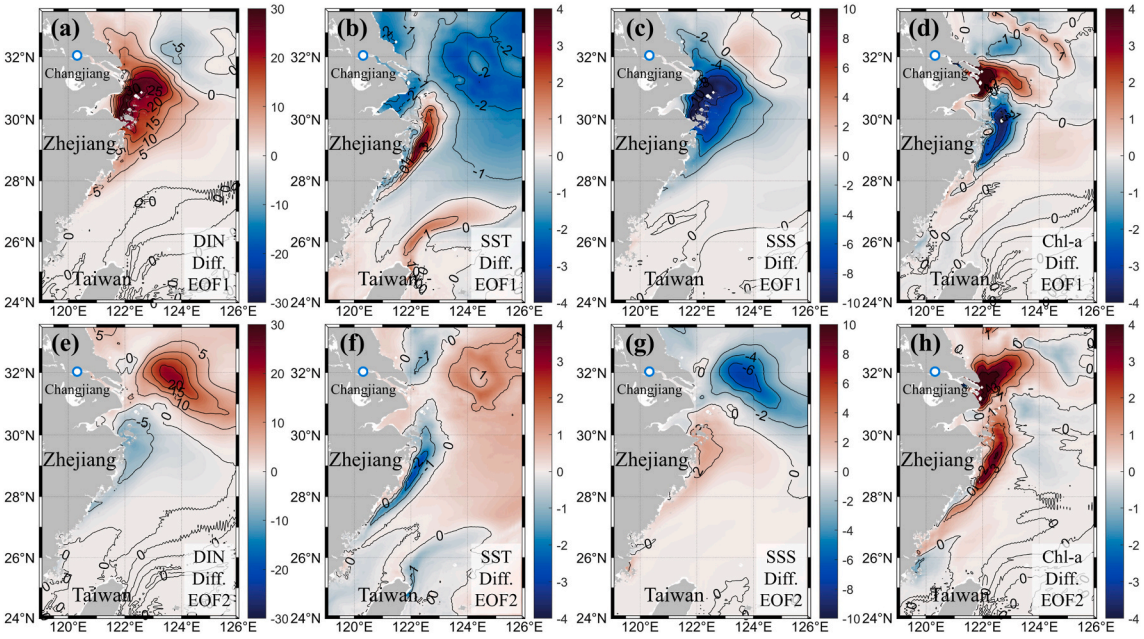

Fig. 8. The differences between the High and Low Maps (Diff. Maps) of DIN concentrations (mmol/m^3), temperatures (T, °C), salinities (S), Chl-a concentrations (mg/m^3) at surface layer for the first EOF mode (EOF1) (a–d) and second EOF mode (EOF2) (e–h) of surface DIN concentrations. For the EOF1, the years to plot the High Maps were 1999, 2002, 2010, 2015, 2019, and 2020, while those for the Low Maps were 1994, 2008, 2009, 2011, and 2013. For the EOF2, the years to plot the High Maps were 1995, 1996, 1998, and 2016, while those for the Low Maps were 2002, 2007, 2015, and 2018.

Based on the aforementioned mechanisms, during high years of the $EOF2_{SN}$ and $EOF2_{SP}$, the stronger ZCU increased DIP supply to the ZC region, stimulated phytoplankton growth and enhanced surface DIN consumption (Figs. 8h and 9h). Concurrently, larger Changjiang discharge and stronger southerly winds drove the CDW northeastward. This offshore extension elevated DIN concentrations offshore (Fig. 8e) and shifted the region of vigorous phytoplankton growth northeastward (Fig. 8h). Consequently, under the high N/P conditions of the CDW, phytoplankton growth led to DIP drawdown (Li et al., 2011), resulting in lower offshore DIP concentrations.

Previous studies have linked ZCU formation to wind fields (Hu and Wang, 2016; Luo et al., 2023). Our results synthesize the controlling role of southerly wind on both ZCU and CDW. The positive correlation (r = 0.82) between meridional wind speed and ZCU intensity indicated that stronger southerly winds simultaneously intensify the ZCU and drive the CDW offshore (as in $EOF2_{SN}$, $EOF2_{SP}$). This wind-driven coordination fundamentally explained the opposing nutrient patterns between offshore and coastal regions in the two dominant modes.

The Diff Map for $EOF1_{BP}$ showed alternating positive/negative signals along the coast of the ZC region, indicating lower bottom DIP shoreward and higher DIP seaward of the ~20 m isobath during high years, a pattern inverse to bottom temperature variations (Fig. 11a and b). The significant correlation between $PC1_{BP}$ and ZCU intensity (Table 1) linked these DIP changes to upwelling dynamics. Analysis of

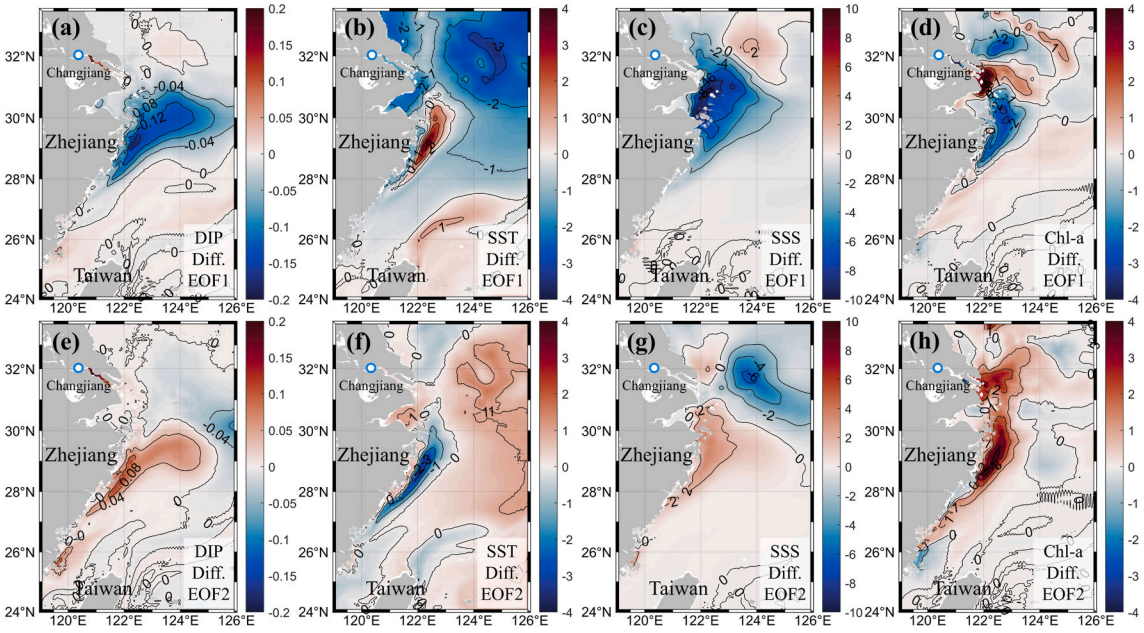

Fig. 9. The differences between the High and Low Maps (Diff. Maps) of DIP concentrations (mmol/m^3), temperatures (T, °C), salinities (S), Chl-a concentrations (mg/m^3) at surface layer for the first EOF mode (EOF1) (a–d) and second EOF mode (EOF2) (e–h) of surface DIP concentrations. For the EOF1, the years to plot the High Maps were 1993, 1999, 2002, 2010, 2015, 2019, and 2020, while those for the Low Maps were 1994, 2000, 2004, 2005, 2013, and 2022. For the EOF2, the years to plot the High Maps were 1995, 1996, 1998, 2003, and 2016, while those for the Low Maps were 2002, 2015, 2018, and 2019.

Diff Maps along Section 122°E (Fig. 12a–d) clarified that weaker ZCU during high years trapped cold, DIP-rich bottom water seaward of the 20-m isobath, reducing shoreward supply and allowing DIP to accumulate offshore. This accumulated water subsequently flowed northward along the isobath, elevating bottom DIP concentrations seaward of the 20-m isobath near the CJE (Fig. 11a).

For EOF2$_{BP}$, its Diff Maps showed uniformly higher bottom DIP concentrations across the ECS shelf during high years (Fig. 11d), coinciding with lower bottom temperatures suggestive of intensified Kuroshio subsurface water intrusion (Yang et al., 2012). The DIP flux across Section B200 (Fig. 1b) (March–June) was calculated to represent Kuroshio intrusion intensity (Luo et al., 2023). Correlation analysis revealed a significant positive relationship ($r = 0.67$, $p < 0.01$) between PC2$_{BP}$ and this intensity index, confirming stronger intrusion during high years. Concurrently, bottom DIP concentrations were elevated along the Kuroshio intrusion path at Section 122°E (Fig. 12e and f). Consequently, the high DIP concentrations originated from increased nutrient supply associated with stronger Kuroshio intrusion.

4.2. *The impacts of ZCU and Kuroshio intrusion on Chl-a concentrations in different regions of the ECS*

To quantify the ecological impacts of the hydrodynamic processes, their relative contributions to phytoplankton biomass (as indicated by Chl-a) were evaluated in two regions: the ZC region and the East Zhejiang coastal (EZC) region (Fig. 1b). The ZCU governs nutrient supply in the ZC region (Yang et al., 2013; Wei et al., 2024), while the Kuroshio intrusion primarily controls nutrient concentrations on the mid- and outer shelf (Chen and Wang, 1999; Xu et al., 2018). In this study, the 30-year water-column-averaged Chl-a concentration in summer in each region calculated and analyzed the relationship with the intensities of the ZCU and Kuroshio intrusion (Fig. 13).

Fig. 13 showed the water-column-averaged Chl-a concentrations in the ZC and EZC regions in July from 1993 to 2022, along with the intensities of the ZCU and the Kuroshio intrusion for each year. The figure was divided into four quadrants using the average ZCU intensity (vertical solid line as the y-axis) and the average Kuroshio intrusion intensity (horizontal solid line as the x-axis). The Quadrant I and III respectively represented the years with strong and weak intensities of both ZCU and Kuroshio intrusion. The Quadrant II represented the years with the weak ZCU intensities and strong Kuroshio intrusion intensities, while the Quadrant IV represented the situation opposite to that of the Quadrant II.

Fig. 13a showed that the average Chl-a concentrations in the ZC region were 1.85 ± 0.34 mg/m^3. The correlation coefficient between the water-column-averaged Chl-a concentrations in the ZC region and the ZCU intensities was 0.60 ($p < 0.01$), while the correlation coefficient with the Kuroshio intrusion intensities was only 0.28 ($p = 0.14$). It was suggested that the ZCU played a dominant role in Chl-a concentrations in the ZC region. The stronger ZCU enhanced the primary production of the ZC region. Additionally, the average values for each year in the four quadrants of the ZC region were 2.12, 1.79, 1.60, and 1.86 mg/m^3, respectively. The maximum value occurred in Quadrant I, including the year 2022 with the highest Chl-a concentrations, while the minimum value occurred in Quadrant III, including the year 2014 with the lowest Chl-a concentrations. It was indicated that both the strong ZCU and Kuroshio intrusion combined to enhance the primary production in the ZC region. Furthermore, there was a nonlinear effect between the ZCU and Kuroshio intrusion intensities. When the ZCU was weak, the Kuroshio intensities increased the Chl-a concentrations by 0.19 mg/m^3 (from Quadrant III to II). In contrast, when the ZCU was strong, the Kuroshio intensities increased the Chl-a concentrations by 0.26 mg/m^3 (from Quadrant IV to I), showing the synergistic effects.

The average Chl-a concentrations in the EZC region were 0.95 ± 0.09 mg/m^3 (Fig. 13b), lower than those in ZC region. The correlation coefficient between the water-column-averaged Chl-a concentrations in the EZC region and the ZCU intensities was −0.32 ($p = 0.09$), while the correlation coefficient with the Kuroshio intrusion intensities was 0.61 ($p < 0.01$). It was suggested that the Kuroshio intrusion played a dominant role in Chl-a concentrations in the EZC region. This aligns with Chen et al. (2021b)'s analysis confirming Kuroshio-derived nutrients as the primary control on shelf productivity. The average values for each year in the four quadrants were 0.95, 1.05, 0.96, and 0.90 mg/m^3, respectively. The maximum value occurred in Quadrant II, including the

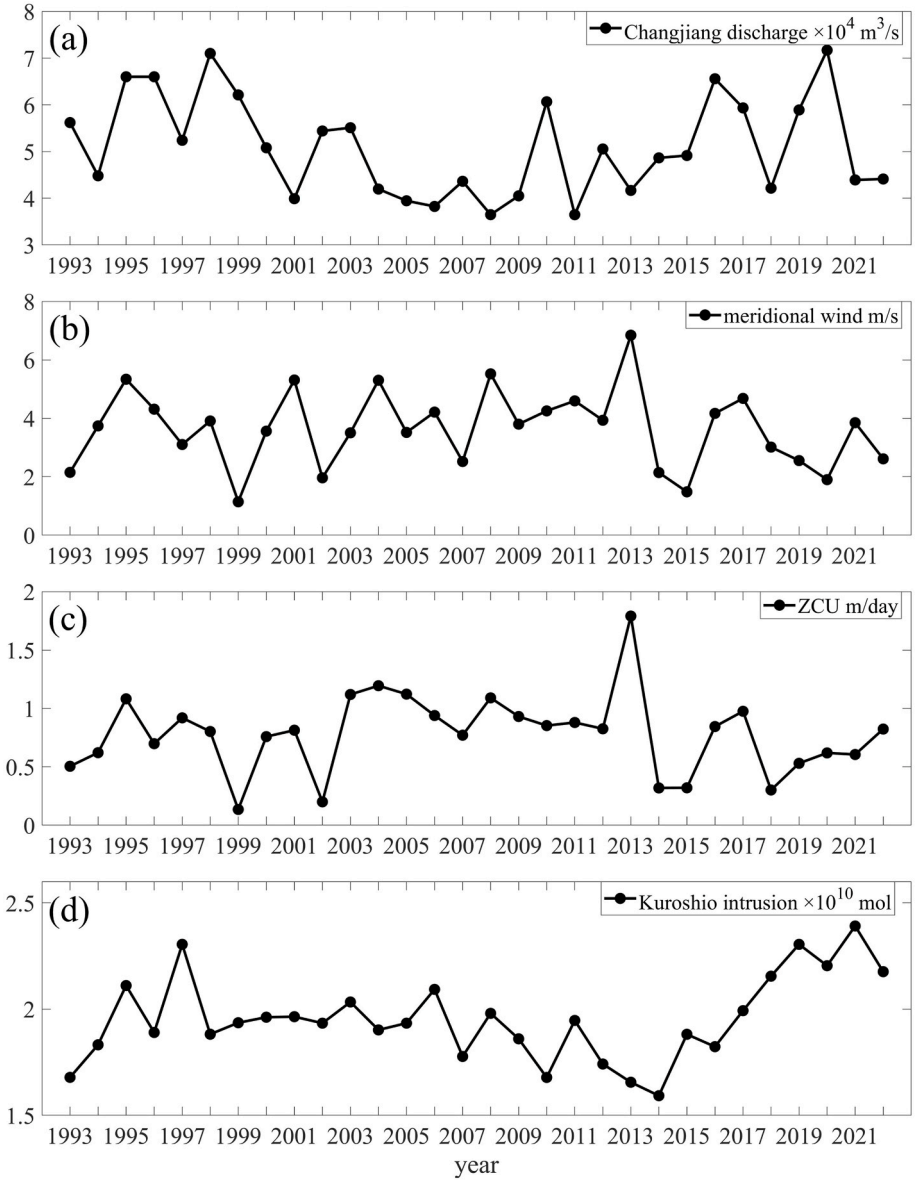

Fig. 10. The interannual variations in (a) Changjiang discharges in July, (b) the average meridional wind in the CJE region in July, (c) the average vertical velocity in the ZC region in July (the ZCU intensity), and (d) the Kuroshio intrusion intensity which was defined by the average DIP flux at the Section B200 from March to June.

Table 1
The correlation coefficient (r) between PC1s of nutrients and hydrodynamic processes.

	ZCU	Changjiang discharge	meridional winds
$PC1_{SN}$	−0.51*	0.74*	−0.61*
$PC1_{SP}$	−0.54*	0.66*	−0.59*
$PC1_{BP}$	−0.65*	0.58*	–

*: $p < 0.05$; the subscript "N" represents DIN, "P" represents DIP, "S" represents the surface layer, and "B" represents the bottom layer.

Table 2
The correlation coefficient (r) between PC2s of nutrients and hydrodynamic processes.

	ZCU	Changjiang discharge	meridional winds
$PC2_{SN}$	0.39*	0.46*	0.50*
$PC2_{SP}$	0.49*	0.43*	0.38*

*: $p < 0.05$; the subscript "N" represents DIN, "P" represents DIP, "S" represents the surface layer, and "B" represents the bottom layer.

year 2020 with the highest Chl-a concentrations, while the minimum value occurred in Quadrant IV, including the year 2004 with the lowest Chl-a concentrations. It was suggested that the Chl-a concentrations in the EZC region were positively influenced by the Kuroshio intrusion, and had a negative correlation with the ZCU. When the Kuroshio intrusion was stronger and the ZCU was weaker, nutrient supplies in the EZC region increased and the primary production was promoted.

It was concluded that in the ZC region, the strong ZCU and Kuroshio intrusion supplied ample nutrients, particularly DIP, to the sea surface. This alleviated local phosphorus limitation and promoted local primary production. In the EZC region, the Kuroshio intrusion offered abundant nutrients that facilitated the growth of phytoplankton. However, the ZCU transported the local DIP-rich seawater to the ZC region, which inhibited local primary production.

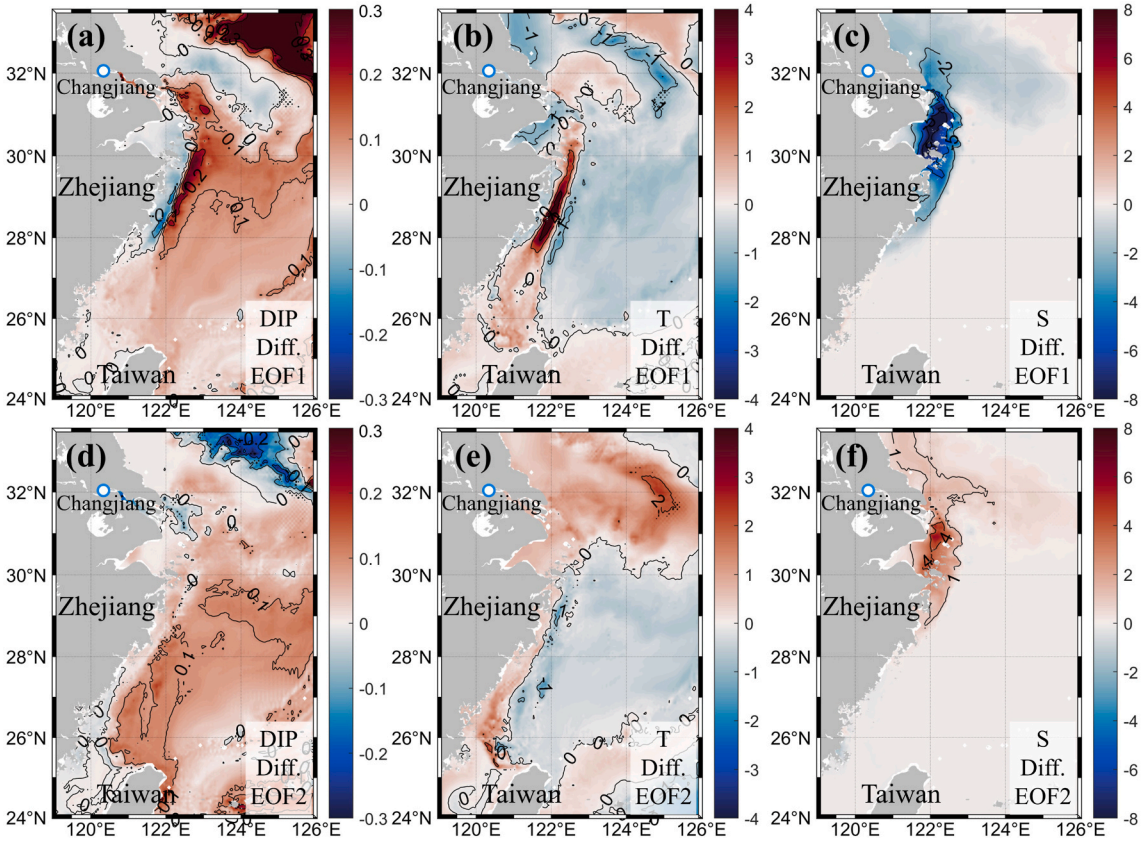

Fig. 11. The differences between the High and Low Maps (Diff.) of DIP concentrations (mmol/m^3), temperatures (T, °C), salinities (S) at bottom layer for the first EOF mode (EOF1) (a–c) and second EOF mode (EOF2) (d–f) of bottom DIP concentrations. For the EOF1, the years to plot the High Maps were 1998, 1999, 2002, 2020, and 2021, while those for the Low Maps were 2004, 2006, 2008, and 2013. For the EOF2, the years to plot the High Maps were 2000, 2006, 2020, 2021, and 2022, while those for the Low Maps were 1993, 2010, and 2016.

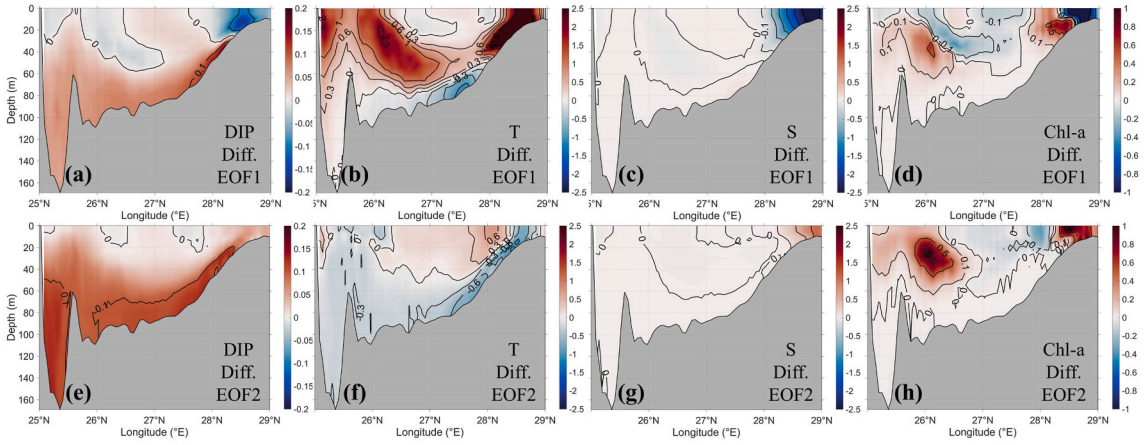

Fig. 12. The differences between the High and Low Maps (Diff.) of DIP concentrations (mmol/m^3), temperatures (T, °C), salinities (S) and Chl-a concentrations (mg/m^3) at Section 122°E for the first EOF mode (EOF1) (a–c) and second EOF mode (EOF2) (d–f) of bottom DIP concentrations.

4.3. Limitations and implications

In this study, the interannual variations of nutrient concentrations were linked to three typical hydrodynamic processes. The riverine input is always attributed to anthropogenic activities, while the intensities of ZCU and Kuroshio represent the natural variations. So, the nutrient input from rivers attracts more attentions because it is regarded to be the only source that can be controlled and consequently plays important role in marine environment management, such as predicting and controlling HABs and seasonal hypoxia (Chai et al., 2006; Qu et al., 2019; Groβe et al., 2020; Zhang et al., 2023). In this study, the sensitive areas influenced by CDW were identified, which will be helpful in controlling the marine environment problems and making nutrient reduction strategies, and finally helps fulfill the coordinated development of land and marine.

There are some limitations of this study. the interannual variations of nutrient inputs from rivers are decided by the riverine concentrations and the water discharge. In the interannual simulations, the interannual

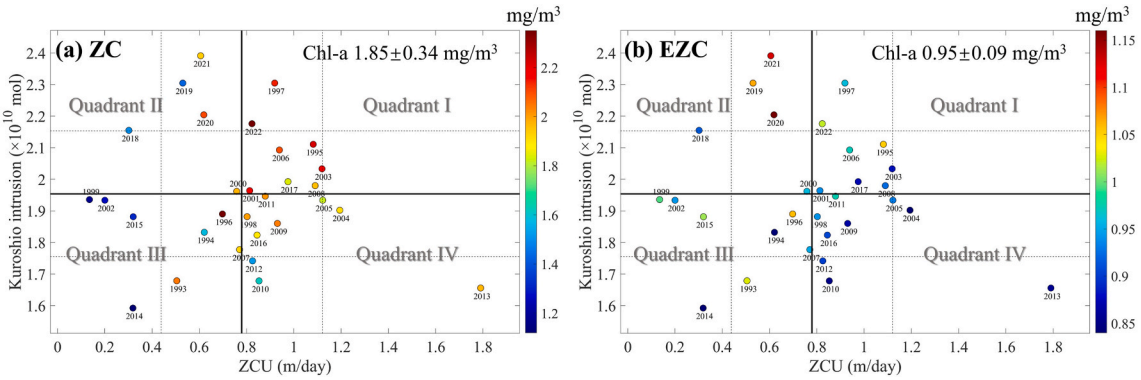

Fig. 13. The Chl-a concentrations in the ZC region (a) and the EZC region (b) during the summer of 1993–2022, as well as the intensities of the ZCU and Kuroshio intrusion. The vertical solid and dashed lines in the figure represent the average ± standard deviation of the ZCU intensities (0.78 ± 0.34 m/day), while the horizontal solid and dashed lines represent the average ± standard deviation of the Kuroshio intrusion intensities (1.95 ± 0.20 × 10^{10} mol DIP).

variations of the freshwater discharge are taken into consideration, while the riverine concentrations are set to be constants. Although, it has been proved by correlation analyses that the interannual variations of fresh water discharge are more important than those of the nutrient concentrations when deciding the interannual variations of the nutrient inputs from rivers, it is still a limitation of this work, more efforts need to be done to reconstruct the long-term variations of riverine nutrient concentrations to evaluated the more reliable effects of rivers.

Besides the river input, there are also other sources of nutrients, such as atmospheric depositions, submarine groundwater discharges, and sediment releases (Zhang et al., 2010; Wang et al., 2018b; Tan et al., 2018; Zhou et al., 2022). Previous studies indicated that their contributions were not as significant as the massive fluxes from the Changjiang River and the Kuroshio intrusion, particularly during the summer high-discharge period (Uno et al., 2007; Wang et al., 2020; Liu et al., 2020). Furthermore, the interannual variability of these fluxes was considerably weaker than that of the wind-driven and river-driven dynamics (Wang et al., 2020). In contrast, sediment resuspension and regeneration were recognized as a major source of nutrients, playing a critical role in the coastal nutrient budget and biogeochemical cycling (Yu et al., 2024; Zhong et al., 2025). Although there are already sediment-water interactions regarding both dissolved and particulate nutrients in the model, the exchanges between water and sediment still need to be quantified in future studies to achieve a more complete understanding of the nutrient dynamics in the ECS.

Moreover, while the EOF analysis has quantitatively assessed the relative importance of these hydrodynamic processes, the isolated contribution of each individual process still needs to be evaluated. Furthermore, climatic events likely drive ECS nutrient variability through remote regulation on the key hydrodynamic processes, while these teleconnections are not evaluated in this study. In future studies, more efforts need to be done on how global climate changes regulate interannual nutrient variabilities in the coastal seas the effects of the climate events based on longer records of data and more scenario-based sensitivity experiments.

5. Conclusion

This study demonstrated that the interannual variability of summer nutrient structure in the ECS was governed by the interplay of three key physical processes: the CDW, the ZCU, and the Kuroshio intrusion. EOF analysis of a 30-year simulation revealed two dominant modes whose alternation was regulated by southerly wind strength, thereby modulating the relative influence of these nutrient sources with contrasting N/P ratios.

The EOF1, characterized by weaker southerly winds and stronger river discharge, favored nearshore retention of the CDW (with a high N/P ratio) and a weakening of the ZCU (with a low N/P ratio). This resulted in the accumulation of surface DIN but a reduction of surface DIP in the ZC region. For bottom waters, the weakened ZCU generated a cross-shore DIP concentration dipole, marked by increases seaward and decreases shoreward of the 20-m isobath.

The EOF2 pattern for surface nutrients was associated with stronger southerly winds. These winds drove the CDW offshore in the CJE region, elevating DIN concentrations there, while simultaneously intensifying the ZCU. This enhanced the supply of DIP in the ZC region, which stimulated phytoplankton growth and led to the consumption and reduction of DIN there. The $EOF2_{BP}$ was primarily linked to the interannual strength of Kuroshio intrusion (with a low N/P ratio), with stronger intrusion leading to a broad increase in bottom DIP concentrations across the shelf.

These distinct nutrient dynamics produced clear regional ecological impacts. Phytoplankton biomass in the ZC region was governed primarily by ZCU intensity, supplemented by nutrients from the Kuroshio intrusion. In contrast, biomass in the offshore EZC region was dominated by the Kuroshio intrusion, which supplied the foundational nutrient reservoir for the mid-shelf.

In summary, this study established a mechanistic framework in which summer southerly wind strength coordinated surface nutrient limitation regimes by regulating the CDW and ZCU, while the Kuroshio intrusion independently governed the bottom DIP reservoir. By linking these coupled physical forcings to nutrient variability, this framework provided a basis for predicting biogeochemical and ecological responses, such as HABs and hypoxia, in the ECS.

CRediT authorship contribution statement

Qingling Zhang: Writing – original draft, Visualization, Validation, Software, Methodology, Investigation, Formal analysis, Data curation, Conceptualization. **Xinyan Mao:** Writing – review & editing, Validation, Software, Methodology, Investigation. **Yifei Luo:** Writing – review & editing, Visualization, Validation, Methodology, Investigation, Conceptualization. **Xinyu Guo:** Supervision, Methodology, Formal analysis. **Jie Shi:** Writing – review & editing, Supervision, Software, Resources, Project administration, Methodology, Investigation, Conceptualization.

Declaration of competing interest

The authors declare that they have no known competing financial interests or personal relationships that could have appeared to influence the work reported in this paper.

Acknowledgments

This study was supported by the National Natural Science Foundation of China (no. 42176022) and the National Key Research and Development Program of China (no. 2023YFF0805001). Q. Zhang was supported by the Ministry of Education, Culture, Sports, Science and Technology, Japan (MEXT) to a project on Joint Usage/Research Center–Leading Academia in Marine and Environment Pollution Research (LaMer).

Appendix A. Supplementary data

Supplementary data to this article can be found online at https://doi.org/10.1016/j.marenvres.2026.107891.

Data availability

Data will be made available on request.

References

Bai, Y., He, X., Pan, D., Chen, C.A., Kang, Y., Chen, X., Cai, W., 2014. Summertime Changjiang River plume variation during 1998–2010. J. Geophys. Res., Oceans 119 (9), 6238–6257. https://doi.org/10.1002/2014jc009866.

Baldacci, A., Corsini, G., Grasso, R., Manzella, G., Allen, J., Cipollini, P., Guymer, T., Snaith, H., 2001. A study of the Alboran sea mesoscale system by means of empirical orthogonal function decomposition of satellite data. J. Mar. Syst. 29 (1–4), 293–311. https://doi.org/10.1016/s0924-7963(01)00021-5.

Blumberg, A.F., Mellor, G.L., 1987. A description of a three-dimensional coastal ocean circulation model. In: Heaps, N.S. (Ed.), Three-Dimensional Coastal Ocean Models, vol. 4. American Geophysical Union, pp. 1–16. https://doi.org/10.1029/co004p0001.

Brzezinski, M.A., Washburn, L., 2011. Phytoplankton primary productivity in the Santa Barbara channel: effects of wind-driven upwelling and mesoscale eddies. J. Geophys. Res. Atmos. 116 (C12), C12013. https://doi.org/10.1029/2011jc007397.

Chabert, P., D'Ovidio, F., Echevin, V., Stukel, M.R., Ohman, M.D., 2021. Cross-shore flow and implications for carbon export in the California current ecosystem: a Lagrangian analysis. J. Geophys. Res., Oceans 126 (2). https://doi.org/10.1029/2020jc016611 e2020JC016611.

Chai, C., Yu, Z., Song, X., Cao, X., 2006. The status and characteristics of eutrophication in the Yangtze River (Changjiang) estuary and the adjacent East China Sea, China. Hydrobiologia 563 (1), 313–328. https://doi.org/10.1007/s10750-006-0021-7.

Chen, C., 1996. The kuroshio intermediate water is the major source of nutrients on the East China Sea continental shelf. Oceanographic Acta 19 (5), 523–527.

Chen, C.A., Wang, S., 1999. Carbon, alkalinity and nutrient budgets on the East China Sea continental shelf. J. Geophys. Res. Atmos. 104 (C9), 20675–20686. https://doi.org/10.1029/1999jc900055.

Chen, C.T.A., Huang, T.H., Wu, C.H., Yang, H., Guo, X., 2021b. Variability of the nutrient stream near Kuroshio's origin. Sci. Rep. 11 (1), 5080. https://doi.org/10.1038/s41598-021-84420-5.

Chen, C., Jan, S., Kuo, T., Li, S., 2017. Nutrient flux and transport by the Kuroshio east of Taiwan. J. Mar. Syst. 167, 43–54. https://doi.org/10.1016/j.jmarsys.2016.11.004.

Chen, C., Shiah, F., Gong, G., Chen, T., 2021a. Impact of upwelling on phytoplankton blooms and hypoxia along the Chinese coast in the East China Sea. Mar. Pollut. Bull. 167, 112288. https://doi.org/10.1016/j.marpolbul.2021.112288.

Chen, Y.L., Chen, H., Gong, G., Lin, Y., Jan, S., Takahashi, M., 2004. Phytoplankton production during a summer coastal upwelling in the East China Sea. Cont. Shelf Res. 24 (12), 1321–1338. https://doi.org/10.1016/j.csr.2004.04.002.

Chi, L., Jiang, K., Ding, Y., Wang, W., Song, X., Yu, Z., 2024. Uncovering nutrient regeneration, transformation pattern, and its contribution to harmful algal blooms in mariculture waters. Sci. Total Environ. 919, 170652. https://doi.org/10.1016/j.scitotenv.2024.170652.

Conley, D.J., Carstensen, J., Ærtebjerg, G., Christensen, P.B., Dalsgaard, T., Hansen, J.L. S., Josefson, A.B., 2007. Long-term changes and impacts of hypoxia in Danish coastal waters. Ecol. Appl. 17 (sp5), S165–S184. https://doi.org/10.1890/05-0766.1.

Gao, L., Li, D., Ishizaka, J., Zhang, Y., Zong, H., Guo, L., 2015. Nutrient dynamics across the river-sea interface in the Changjiang (Yangtze River) estuary-East China sea region. Limnol. Oceanogr. 60 (6), 2207–2221. https://doi.org/10.1002/lno.10196.

Große, F., Fennel, K., Zhang, H., Laurent, A., 2020. Quantifying the contributions of riverine vs. oceanic nitrogen to hypoxia in the East China Sea. Biogeosciences 17 (10), 2701–2714. https://doi.org/10.5194/bg-17-2701-2020.

Guillaud, J., Aminot, A., Delmas, D., Gohin, F., Lunven, M., Labry, C., Herbland, A., 2008. Seasonal variation of riverine nutrient inputs in the northern Bay of Biscay (France), and patterns of marine phytoplankton response. J. Mar. Syst. 72 (1–4), 309–319. https://doi.org/10.1016/j.jmarsys.2007.03.010.

Guo, S., Feng, Y., Wang, L., Dai, M., Liu, Z., Bai, Y., Sun, J., 2014. Seasonal variation in the phytoplankton community of a continental-shelf sea: the East China Sea. Mar. Ecol. Prog. Ser. 516, 103–126. https://doi.org/10.3354/meps10952.

Guo, X., Miyazawa, Y., Yamagata, T., 2006. The Kuroshio onshore intrusion along the shelf break of the East China Sea: the origin of the tsushima warm current. J. Phys. Oceanogr. 36 (12), 2205–2231. https://doi.org/10.1175/jpo2976.1.

Heinze, C., 2014. The role of the ocean carbon cycle in climate change. Eur. Rev. 22 (1), 97–105. https://doi.org/10.1017/s1062798713000665.

Hou, W., Ba, M., Bai, J., Yu, J., 2021. Numerical study on the expansion and variation of changjiang diluted water in summer and autumn. J. Mar. Sci. Eng. 9 (3), 317. https://doi.org/10.3390/jmse9030317.

Hu, J., Wang, X.H., 2016. Progress on upwelling studies in the China seas. Rev. Geophys. 54 (3), 653–673. https://doi.org/10.1002/2015rg000505.

Jiang, Z., Chen, J., Zhou, F., Shou, L., Chen, Q., Tao, B., Yan, X., Wang, K., 2015. Controlling factors of summer phytoplankton community in the Changjiang (Yangtze River) Estuary and adjacent East China Sea shelf. Cont. Shelf Res. 101, 71–84. https://doi.org/10.1016/j.csr.2015.04.009.

Kim, J., Chapman, P., Rowe, G., DiMarco, S.F., 2020. Categorizing zonal productivity on the continental shelf with nutrient-salinity ratios. J. Mar. Syst. 206, 103336. https://doi.org/10.1016/j.jmarsys.2020.103336.

Li, D., Chen, J., Wang, B., Jin, H., Shou, L., Lin, H., Miao, Y., Sun, Q., Jiang, Z., Meng, Q., Zeng, J., Zhou, F., Cai, W., 2024a. Hypoxia triggered by expanding river plume on the East China Sea inner shelf during flood years. J. Geophys. Res., Oceans 129 (8). https://doi.org/10.1029/2024jc021299 e2024JC021299.

Li, S., Zhong, Y., Zhou, M., Wu, H., Gao, Y., Zhou, P., Wang, Y., Zhang, Z., Zhang, H., 2024b. The summer Kuroshio intrusion into the East China Sea revealed by a new mixed-layer water mass analysis. J. Geophys. Res., Oceans 129 (4). https://doi.org/10.1029/2023jc020827 e2023JC020827.

Li, X., Yu, Z., Song, X., Cao, X., Yuan, Y., 2011. Nitrogen and phosphorus budgets of the changjiang River estuary. Chin. J. Oceanol. Limnol. 29 (4), 762–774. https://doi.org/10.1007/s00343-011-0505-9.

Liang, C., Xian, W., 2018. Changjiang nutrient distribution and transportation and their impacts on the estuary. Cont. Shelf Res. 165, 137–145. https://doi.org/10.1016/j.csr.2018.05.001.

Lin, F., Liang, C., Ding, T., Zeng, D., Zhou, F., Ma, X., Yang, C., Li, H., Zhou, B., Liu, C., Jin, W., 2023. A preliminary Study of suspended matters variation associated with hypoxia and shoaling internal tides on the Continental shelf of the Northern andaman sea. J. Mar. Sci. Eng. 11 (10), 1950. https://doi.org/10.3390/jmse11101950.

Liu, K., Chao, S., Lee, H., Gong, G., Teng, Y., 2010. Seasonal variation of primary productivity in the East China Sea: a numerical study based on coupled physical-biogeochemical model. Deep Sea Res. Part II Top. Stud. Oceanogr. 57 (19–20), 1762–1782. https://doi.org/10.1016/j.dsr2.2010.04.003.

Liu, S.M., Ning, X., Dong, S., Song, G., Wang, L., Altabet, M.A., Zhu, Z., Wu, Y., Ren, J.L., Liu, C.G., Zhang, J., Huang, D., 2020. Source versus recycling influences on the isotopic composition of nitrate and nitrite in the East China Sea. J. Geophys. Res., Oceans 125 (8). https://doi.org/10.1029/2020jc016061.

Liu, S.M., Qi, X.H., Li, X., Ye, H.R., Wu, Y., Ren, J.L., Zhang, J., Xu, W.Y., 2016. Nutrient dynamics from the Changjiang (Yangtze River) estuary to the East China Sea. J. Mar. Syst. 154, 15–27. https://doi.org/10.1016/j.jmarsys.2015.05.010.

Liu, W., Song, J., Yuan, H., Li, N., Li, X., Duan, L., 2017. Dissolved barium as a tracer of Kuroshio incursion in the Kuroshio region east of Taiwan island and the adjacent East China Sea. Sci. China Earth Sci. 60 (7), 1356–1367. https://doi.org/10.1007/s11430-016-9039-7.

Liu, X., Beusen, A.H., Van Beek, L.P., Mogollón, J.M., Ran, X., Bouwman, A.F., 2018. Exploring spatiotemporal changes of the Yangtze River (Changjiang) nitrogen and phosphorus sources, retention and export to the East China Sea and yellow sea. Water Res. 142, 246–255. https://doi.org/10.1016/j.watres.2018.06.006.

Luo, X., Jiao, J.J., Liu, Y., Zhang, X., Liang, W., Tang, D., 2018. Evaluation of water residence time, submarine groundwater discharge, and maximum new production supported by groundwater borne nutrients in a coastal upwelling shelf system. J. Geophys. Res., Oceans 123 (1), 631–655. https://doi.org/10.1002/2017jc013398.

Luo, Y., Shi, J., Guo, X., Mao, X., Yao, P., Zhao, B., Chen, L., Wang, Y., 2023. Yearly variations in nutrient supply in the East China Sea due to the Zhejiang coastal upwelling and Kuroshio intrusion. J. Geophys. Res., Oceans 128 (4). https://doi.org/10.1029/2022jc019216 e2022JC019216.

Lyu, W., Sun, Q., Wang, S., Li, B., 2020. Summer vertical turbulent nitrate flux in the yellow sea and the East China Sea. Oceanol. Limnol. Sinica 51 (6), 1379–1390. https://doi.org/10.11693/hyhz20200100033.

Mellor, G., 2003. The three-dimensional current and surface wave equations. J. Phys. Oceanogr. 33 (9), 1978–1989. https://doi.org/10.1175/1520-0485(2003)033.

Mi, T., Yao, Q., M, J., Zhang, X., Liu, S., 2012. Distributions of nutrients in the southern yellow sea and East China Sea in spring and summer 2011. Oceanol. Limnol. Sinica 43 (3), 678–688. https://doi.org/10.11693/hyhz201203040040.

Miyazawa, Y., Zhang, R., Guo, X., Tamura, H., Ambe, D., Lee, J., Okuno, A., Yoshinari, H., Setou, T., Komatsu, K., 2009. Water mass variability in the Western North Pacific detected in a 15-year eddy resolving ocean reanalysis. J. Oceanogr. 65 (6), 737–756. https://doi.org/10.1007/s10872-009-0063-3.

Moon, J., Hirose, N., Pang, I., Hyun, K.H., 2012. Modeling offshore freshwater dispersal from the Changjiang River and controlling factors during summer. Terr. Atmos. Ocean Sci. 23 (3), 247. https://doi.org/10.3319/TAO.2012.01.10.01(Oc.

Peng, P., Bi, R., Sachs, J.P., Shi, J., Luo, Y., Chen, W., Huh, C., Yu, M., Cao, Y., Wang, Y., Cao, Z., Bao, X., Guo, X., Li, H., Feng, X., Li, H., Zhao, M., 2023. Phytoplankton community changes in a coastal upwelling system during the last century. Global Planet. Change 224, 104101. https://doi.org/10.1016/j.gloplacha.2023.104101.

Pereira, A., Belém, A., Castro, B.M., Geremias, R., 2005. Tide-topography interaction along the eastern Brazilian shelf. Cont. Shelf Res. 25 (12–13), 1521–1539. https://doi.org/10.1016/j.csr.2005.04.008.

Qu, D., Yu, H., Sun, Y., Zhao, Y., Wei, Q., Yu, H., Kelly, R.M., Yuan, Y., 2019. Numerical study on the summertime patches of red tide in the adjacent sea of the Changjiang (Yangtze) River Estuary, China. Mar. Pollut. Bull. 143, 242–255. https://doi.org/10.1016/j.marpolbul.2019.04.027.

Rabouille, C., Conley, D., Dai, M., Cai, W., Chen, C., Lansard, B., Green, R., Yin, K., Harrison, P., Dagg, M., McKee, B., 2008. Comparison of hypoxia among four river-dominated ocean margins: the Changjiang (Yangtze), Mississippi, pearl, and Rhône rivers. Cont. Shelf Res. 28 (12), 1527–1537. https://doi.org/10.1016/j.csr.2008.01.020.

Rattanarat, J., Jaroensutasinee, M., Jaroensutasinee, K., Sawasdee, A., Sparrow, E.B., 2024. Nursery habitat requirements for the blue swimming crab: implications for larval development. J. Hum. Earth Future 5 (3), 306–318. https://doi.org/10.28991/hef-2024-05-03-01.

Siswanto, E., Nakata, H., Matsuoka, Y., Tanaka, K., Kiyomoto, Y., Okamura, K., Zhu, J., Ishizaka, J., 2008. The long-term freshening and nutrient increases in summer surface water in the northern East China Sea in relation to Changjiang discharge variation. J. Geophys. Res. Atmos. 113 (C10). https://doi.org/10.1029/2008jc004812.

Skogen, M.D., Søiland, H., 1998. A User's Guide to NORWECOM v2.0. the Norwegian Ecological Model System. Institute of Marine Research.

Sudheesh, V., Movitha, M., Hatha, A.M., Renjith, K., Resmi, P., Rahiman, M., Nair, S., 2017. Effects of seasonal anoxia on the distribution of phosphorus fractions in the surface sediments of southeastern Arabian Sea shelf. Cont. Shelf Res. 150, 57–64. https://doi.org/10.1016/j.csr.2017.09.011.

Sun, Q., Li, D., Wang, B., Xu, Z., Miao, Y., Lin, H., Jin, H., Jiang, Z., Zeng, J., Zhou, F., Chen, J., 2023. Massive nutrients offshore transport off the Changjiang Estuary in flooding summer of 2020. Front. Mar. Sci. 10. https://doi.org/10.3389/fmars.2023.1076336.

Tan, E., Wang, G., Moore, W.S., Li, Q., Dai, M., 2018. Shelf-scale submarine groundwater discharge in the Northern South China Sea and East China Sea and its geochemical impacts. J. Geophys. Res., Oceans 123 (4), 2997–3013. https://doi.org/10.1029/2017jc013405.

Tseng, Y., Lin, J., Dai, M., Kao, S., 2014. Joint effect of freshwater plume and coastal upwelling on phytoplankton growth off the Changjiang River. Biogeosciences 11 (2), 409–423. https://doi.org/10.5194/bg-11-409-2014.

Uno, I., Uematsu, M., Hara, Y., He, Y.J., Ohara, T., Mori, A., Kamaya, T., Murano, K., Sadanaga, Y., Bandow, H., 2007. Numerical study of the atmospheric input of anthropogenic total nitrate to the marginal seas in the Western North Pacific region. Geophys. Res. Lett. 34 (17). https://doi.org/10.1029/2007gl030338.

Wang, B., Wang, X., 2007. Chemical hydrography of coastal upwelling in the East China Sea. Chin. J. Oceanol. Limnol. 25 (1), 16–26. https://doi.org/10.1007/s00343-007-0016-x.

Wang, H., Bouwman, A.F., Wang, J., Yu, Z., Ran, X., 2023. Competitive advantages of HAB species under changing environmental conditions in the coastal waters of the Bohai Sea, Yellow sea and East China Sea. Cont. Shelf Res. 259, 104991. https://doi.org/10.1016/j.csr.2023.104991.

Wang, J., Beusen, A.H.W., Liu, X., Van Dingenen, R., Dentener, F., Yao, Q., Xu, B., Ran, X., Yu, Z., Bouwman, A.F., 2020. Spatially explicit inventory of sources of nitrogen inputs to the Yellow sea, East China Sea, and South China Sea for the period 1970–2010. Earths Future 8 (10). https://doi.org/10.1029/2020ef001516.

Wang, K., Yin, K., 2021. Barrier effect of the Pearl River estuarine plume on wind-induced coastal upwelling of nutrients. J. Geophys. Res. Biogeosci. 126 (11). https://doi.org/10.1029/2020jg006067 e2020JG006067.

Wang, K., Chen, J., Jin, H., Chen, F., Li, H., Gao, S., Lu, Y., 2011. The four seasons nutrients distribution in Changjiang River Estuary and its adjacent East China Sea. J. Marine Sci. 29 (3), 18–35. https://doi.org/10.3969/j.issn.1001-909X.2011.03.004.

Wang, Q., Guo, X., Takeoka, H., 2008. Seasonal variations of the Yellow River plume in the Bohai Sea: a model study. J. Geophys. Res. Atmos. 113 (C8), C08046. https://doi.org/10.1029/2007jc004555.

Wang, W., Yu, Z., Song, X., Chi, L., Zhou, P., Wu, Z., Yuan, Y., 2022. Hypoxia formation in the East China Sea by decomposed organic matter in the Kuroshio subsurface water. Mar. Pollut. Bull. 177, 113486. https://doi.org/10.1016/j.marpolbul.2022.113486.

Wang, X., Baskaran, M., Su, K., Du, J., 2018b. The important role of submarine groundwater discharge (SGD) to derive nutrient fluxes into river dominated ocean margins – the East China Sea. Mar. Chem. 204, 121–132. https://doi.org/10.1016/j.marchem.2018.05.010.

Wang, X., Liu, J., Zhang, R., Zhang, Y., Zhou, Z., Han, Q., 2024. Trend and interannual variability of summer marine heatwaves in the tropical Indian ocean: patterns, mixed layer heat budget, and seasonal prediction. Weather Clim. Extrem. 44, 100680. https://doi.org/10.1016/j.wace.2024.100680.

Wang, Y., Guo, X., Zhao, L., 2018a. Simulating the responses of a low-trophic ecosystem in the East China Sea to decadal changes in nutrient load from the Changjiang (Yangtze) River. J. Oceanol. Limnol. 36 (1), 48–61. https://doi.org/10.1007/s00343-017-6233-z.

Wang, Y., Guo, X., Zhao, L., Zhang, J., 2019. Seasonal variations in nutrients and biogenic particles in the upper and lower layers of East China Sea shelf and their export to adjacent seas. Prog. Oceanogr. 176, 102138. https://doi.org/10.1016/j.pocean.2019.102138.

Wang, Y., Xu, H., Li, M., 2021. Long-term changes in phytoplankton communities in China's Yangtze Estuary driven by altered riverine fluxes and rising sea surface temperature. Geomorphology 376, 107566. https://doi.org/10.1016/j.geomorph.2020.107566.

Wei, Q., Xin, M., Meng, Q., Zhao, B., Teng, F., Xie, L., Zhai, X., Sun, X., Zhou, F., Wang, B., 2024. Upwelling regulates nutrient supply and phytoplankton chlorophyll-A regime on the East China Sea shelf during late summer. J. Geophys. Res., Oceans 129 (8). https://doi.org/10.1029/2023jc020569 e2023JC020569.

Wei, Q., Yao, P., Xu, B., Zhao, B., Ran, X., Zhao, Y., Sun, J., Wang, B., Yu, Z., 2021. Coastal upwelling combined with the river plume regulates hypoxia in the Changjiang estuary and adjacent inner East China Sea shelf. J. Geophys. Res., Oceans 126 (11). https://doi.org/10.1029/2021jc017740.

Wu, H., Yang, W., Zhang, W., Zhao, X., 2023. Changjiang and Kuroshio contributions to oxygen depletion on the Zhejiang Coast. Front. Mar. Sci. 10. https://doi.org/10.3389/fmars.2023.1285426.

Xiao, T., Feng, J., Qiu, Z., Tang, R., Zhao, A., Wong, K., Tsou, J.Y., Zhang, Y., 2024. Remote-sensing estimation of upwelling-frequent areas in the adjacent waters of Zhoushan (China). J. Mar. Sci. Eng. 12 (7), 1085. https://doi.org/10.3390/jmse12071085.

Xu, L., Yang, D., Benthuysen, J.A., Yin, B., 2018. Key dynamical factors driving the Kuroshio subsurface water to reach the Zhejiang coastal area. J. Geophys. Res., Oceans 123 (12), 9061–9081. https://doi.org/10.1029/2018jc014219.

Xu, Y., Ishizaka, J., Yamaguchi, H., Siswanto, E., Wang, S., 2013. Relationships of interannual variability in SST and phytoplankton blooms with giant jellyfish (Nemopilema nomurai) outbreaks in the Yellow Sea and East China Sea. J. Oceanogr. 69 (5), 511–526. https://doi.org/10.1007/s10872-013-0189-1.

Yang, D., Yin, B., Chai, F., Feng, X., Xue, H., Gao, G., Yu, F., 2018. The onshore intrusion of Kuroshio subsurface water from February to July and a mechanism for the intrusion variation. Prog. Oceanogr. 167, 97–115. https://doi.org/10.1016/j.pocean.2018.08.004.

Yang, D., Yin, B., Liu, Z., Bai, T., Qi, J., Chen, H., 2012. Numerical study on the pattern and origins of Kuroshio branches in the bottom water of southern East China Sea in summer. J. Geophys. Res. Atmos. 117 (C2), C02014. https://doi.org/10.1029/2011jc007528.

Yang, D., Yin, B., Sun, J., Zhang, Y., 2013. Numerical study on the origins and the forcing mechanism of the phosphate in upwelling areas off the coast of Zhejiang province, China in summer. J. Mar. Syst. 123–124, 1–18. https://doi.org/10.1016/j.jmarsys.2013.04.002.

Yang, L., Zhang, J., Yang, G., 2021. Mixing behavior, biological and photolytic degradation of dissolved organic matter in the East China Sea and the Yellow Sea. Sci. Total Environ. 762, 143164. https://doi.org/10.1016/j.scitotenv.2020.143164.

Ye, L., Wang, L., Jiang, Z., Lu, S., Zhu, Z., Li, D., 2017. Seasonal variations of distribution characteristics of nutrients in the East China Sea in 2015. J. Shanghai Ocean Univ. 26 (3), 432–439. https://doi.org/10.12024/jsou.20160801846.

Ye, R., Liu, Y., Cui, Y., Wang, Z., Ye, X., 2015. Temporal and spatial distributions of nutrient structure and limitation on phytoplankton in the East China Sea. Oceanol. Limnol. Sinica 46 (2), 311–320. https://doi.org/10.11693/hyhz20140400122.

Yu, X., Liu, J., Wang, X., Chen, X., Du, J., 2024. Unveiling the dominance of submarine groundwater discharge on nutrient sources in the eastern China marginal seas. Water Res. 262, 122136. https://doi.org/10.1016/j.watres.2024.122136.

Yuan, N., Mitsudera, H., 2023. Cross-shelf overturning in geostrophic-stress-dominant coastal fronts. J. Oceanogr. 79 (1), 27–48. https://doi.org/10.1007/s10872-022-00661-6.

Zhang, J., Guo, X., Zhao, L., 2019. Tracing external sources of nutrients in the East China Sea and evaluating their contributions to primary production. Prog. Oceanogr. 176, 102122. https://doi.org/10.1016/j.pocean.2019.102122.

Zhang, W., Luo, D., 2024. The variability of winter North Atlantic blocking and cold extremes connected to North Atlantic Sea surface temperature modes and ENSO: the mediated role of North Atlantic jet. Atmos. Res. 297, 107092. https://doi.org/10.1016/j.atmosres.2023.107092.

Zhang, W., Zhou, F., Huang, D., Chen, J., Zhu, J., 2023. Mechanisms controlling interannual variability of seasonal hypoxia off the Changjiang River Estuary. J. Geophys. Res., Oceans 128 (10). https://doi.org/10.1029/2023jc019996 e2023JC019996.

Zhang, X., Fan, D., Wang, H., Yang, Z., 2014. Water discharge variability of Changjiang (Yangtze) and Huanghe (Yellow) Rivers and its response to climatic changes. Chin. J. Oceanol. Limnol. 32 (6), 1392–1405. https://doi.org/10.1007/s00343-015-4034-9.

Zhang, Y., Yu, Q., Ma, W., Chen, L., 2010. Atmospheric deposition of inorganic nitrogen to the eastern China seas and its implications to marine biogeochemistry. J. Geophys. Res. Atmos. 115 (D7). https://doi.org/10.1029/2009jd012814.

Zhao, L., Guo, X., 2011. Influence of cross-shelf water transport on nutrients and phytoplankton in the East China Sea: a model study. Ocean Sci. 7 (1), 27–43. https://doi.org/10.5194/os-7-27-2011.

Zhong, X., Liu, J., Shi, M., Liu, X., Lv, Z., Ran, X., 2025. Nutrient dynamics in the East China Sea: seasonal changes, budget, and ecological impacts. Prog. Oceanogr. 234, 103463. https://doi.org/10.1016/j.pocean.2025.103463.

Zhou, N., Zhang, G.L., Liu, S.M., 2022. Nutrient exchanges at the sediment-water interface and the responses to environmental changes in the Yellow Sea and East China Sea. Mar. Pollut. Bull. 176, 113420. https://doi.org/10.1016/j.marpolbul.2022.113420.

Zhou, P., Song, X., Yuan, Y., Wang, W., Chi, L., Cao, X., Yu, Z., 2018. Intrusion of the Kuroshio subsurface water in the southern East China Sea and its variation in 2014 and 2015 traced by dissolved inorganic iodine species. Prog. Oceanogr. 165, 287–298. https://doi.org/10.1016/j.pocean.2018.06.011.